AD_____

Award Number: W81XWH-08-1-0367

TITLE:

Regulatory Role of the NF-kB Pathway in Lymphangiogenesis and Breast Cancer Metastasis

PRINCIPAL INVESTIGATOR:
Michael Flister, B.S.

CONTRACTING ORGANIZATION:
Southern Illinois University School of Medicine, Springfield, IL, 62702

REPORT DATE:
July 2010

TYPE OF REPORT:
Annual Summary

PREPARED FOR: U.S. Army Medical Research and Materiel Command
Fort Detrick, Maryland 21702-5012

DISTRIBUTION STATEMENT:

√ Approved for public release; distribution unlimited

REPORT DOCUMENTATION PAGE

Form Approved
OMB No. 0704-0188

1. REPORT DATE	2. REPORT TYPE	3. DATES COVERED *(From - To)*
01-07-2010	Annual Summary	1 Jul 2009 – 30 Jun 2010

4. TITLE AND SUBTITLE

Regulatory Role of the NF-kB Pathway in Lymphangiogenesis and Breast Cancer Metastasis

5a. CONTRACT NUMBER

5b. GRANT NUMBER
W81XWH-08-1-0367

5c. PROGRAM ELEMENT NUMBER

6. AUTHOR(S)
Mike Flister (PI); Sophia Ran, PhD (Mentor)

5d. PROJECT NUMBER

5e. TASK NUMBER

5f. WORK UNIT NUMBER

7. PERFORMING ORGANIZATION NAME(S) AND ADDRESS(ES)
Southern Illinois University School of Medicine

Springfield, IL, 62702

8. PERFORMING ORGANIZATION REPORT NUMBER

9. SPONSORING / MONITORING AGENCY NAME(S) AND ADDRESS(ES)
U.S. Army Medical Research and Material Command
Fort Detrick, Maryland 21702-5012

10. SPONSOR/MONITOR'S ACRONYM(S)

11. SPONSOR/MONITOR'S REPORT NUMBER(S)

12. DISTRIBUTION / AVAILABILITY STATEMENT
Approved for public release; distribution unlimited

13. SUPPLEMENTARY NOTES

14. ABSTRACT

Abstract on next page.

15. SUBJECT TERMS
Breast cancer metastasis; Lymphatic; Lymphangiogenesis; Vascular endothelial growth factor receptor-3 (VEGFR-3); Prospero-related homeobox-1 (Prox1); Inflammation; Nuclear factor-kappa B (NF-κB)

16. SECURITY CLASSIFICATION OF:			17. LIMITATION OF ABSTRACT	18. NUMBER OF PAGES	19a. NAME OF RESPONSIBLE PERSON
a. REPORT	b. ABSTRACT	c. THIS PAGE			USAMRMC
U	U	U	UU	46	19b. TELEPHONE NUMBER *(include area code)*

14. ABSTRACT

Elevation of VEGFR-3, the primary mediator of lymphangiogenesis (i.e., new lymphatic vessel formation), is frequently associated with inflammation related to chronic disease and cancer. In the latter case, VEGFR-3 dependent lymphangiogenesis induced by inflamed tumors increases the incidence of distant metastasis, leading to decreased patient survival. However, the molecular mechanisms underlying inflammation-induced VEGFR-3 elevation and lymphangiogenesis are currently unknown. Two potential candidate genes that may regulate expression of VEGFR-3 are Prox1, the primary mediator of embryonic lymphangiogenesis, and NF-κB, the key intracellular regulator of inflammation-induced transcription. We hypothesized that the key inflammatory mediator, NF-κB, regulates transcription of key mediators of lymphangiogenesis, VEGFR-3 and Prox1. We further hypothesized that inflammation-induced elevation of VEGFR-3 and Prox1 are essential steps required for robust lymphangiogenesis in response to inflammation. The three primary goals of this study were to (1) delineate the time-course of events leading to inflammation-induced lymphangiogenesis *in vivo*; (2) clone and characterize the VEGFR-3 promoter and identify factors regulating VEGFR-3 expression *in vitro*; and (3) characterize the lymphatic phenotype of NF-κB p50 knockout mice.

To begin testing these hypotheses, we used a mouse model of peritonitis to characterize induction of lymphangiogenesis and expression kinetics of NF-κB, Prox1 and VEGFR-3. *In vivo* time-course analysis of inflammation-induced lymphangiogenesis showed activation of NF-κB followed by sequential upregulation of Prox1 and VEGFR-3 that preceded lymphangiogenesis by 4 and 2 days, respectively. Characterization of the VEGFR-3 promoter by luciferase-reporter and ChIP assays showed direct activation by Prox1, NF-κB p50 and p65 transcription factors. This also revealed that Prox1 and NF-κB p50 bind in close proximity and synergistically activate the VEGFR-3 promoter. Characterization of p50 knockout mice revealed significantly decreased lymphatic vessel density in several organs that corresponded to reduced VEGFR-3 and Prox1 expression. Activation of NF-κB by inflammatory stimuli also elevated expression of NF-κB, Prox1 and VEGFR-3 in cultured lymphatic endothelial cells, which enhanced proliferation and migration in response to the VEGFR-3-specific ligand, VEGF-C152S. Collectively, our findings suggest that induction of the NF-κB pathway by inflammatory stimuli activates Prox1, and both NF-κB and Prox1 activate the VEGFR-3 promoter leading to increased receptor expression in lymphatic endothelial cells. This, in turn, enhances the responsiveness of pre-existing lymphatic endothelium to VEGFR-3 binding factors, VEGF-C and VEGF-D, ultimately resulting in robust lymphangiogenesis.

Table of Contents

Page

Introduction:

Chronic inflammation is frequently associated with breast cancer development[1;2], progression, and metastasis, which is the leading cause of mortality in these patients[3]. Frequently, the formation of new lymphatic vessels, i.e., lymphangiogenesis, facilitates initial metastasis to regional lymph nodes. Strong correlative evidence links chronic inflammation to both increased lymphangiogenesis[4] and breast cancer metastasis[5], but the direct mechanism(s) are largely unknown. The key protein that regulates lymphangiogenesis is vascular endothelial growth factor receptor-3 (VEGFR-3)[6], a tyrosine kinase receptor expressed primarily in lymphatic endothelial cells (LECs)[7]. VEGFR-3 signaling is activated upon binding of vascular endothelial growth factor (VEGF)-C or the related factor, VEGF-D[6]. In adulthood, lymphangiogenesis and elevated VEGFR-3 expression coincide with pro-inflammatory conditions including cancer[8], wound healing[9], and chronic inflammatory diseases. Increased lymphatic vessel density has been documented in chronic airway infection[10], psoriasis[11], arthritis[12] and corneal injury[13]. VEGF-C and VEGF-D are elevated during inflammation, being produced by a variety of cells residing at inflamed sites, including macrophages[10;14;15], dendritic cells, neutrophils[10], mast cells, fibroblasts[16] and tumor cells[15]. Inflammation-induced lymphatic hyperplasia and lymphangiogenesis are likely the result of increased VEGFR-3 expression that amplifies response to VEGF-C/-D. This is supported by observations that blocking VEGFR-3 signaling inhibits lymphangiogenesis during chronic inflammation[10], wound healing[17], and malignancy[18]. Lymphangiogenesis is also regulated by the lymphatic-specific transcription factor, Prospero-related homeobox-1 (Prox1)[19;20] that specifies lymphatic endothelial cell-fate by regulating VEGFR-3[20] and other lymphatic-specific proteins during embryogenesis. The central role of Prox1 in developmental lymphangiogenesis suggests a similar role for Prox1 in adulthood. Studies have shown that Prox1 induces VEGFR-3 expression in adult blood vascular endothelial cells (BECs)[19;21], whereas silencing Prox1 in adult LECs downregulates VEGFR-3 expression[21;22]. Prox1 has been shown to be upregulated by inflammatory cytokines[23] and to colocalize with VEGFR-3 in lymphatic vessels. However, the role of Prox1 in regulation of VEGFR-3 expression during inflammation *in vivo* is unknown. The primary mediators of the intracellular response to inflammation are dimeric transcription factors that belong to the nuclear factor-kappaB (NF-κB)

family consisting of RelA (p65), NF-κB1 (p50), RelB, c-Rel, and NF-κB2 (p52)[24]. The main NF-κB protein complexes that regulate the transcription of responsive genes are p50/p65 heterodimers or p50 and p65 homodimers[25]. Over 450 NF-κB inducible genes have been identified, including proteins that mediate inflammation, immunity, tumorigenesis, and angiogenesis[24]. Several NF-κB-regulated genes stimulate lymphangiogenesis either directly (e.g., VEGF-A[26] and VEGF-C[27]) or indirectly, by upregulating VEGF-C and VEGF-D (e.g., IL-1β[16], TNF-α[16]and COX-2[15]). Activated NF-κB signaling coincides with increased VEGFR-3$^+$ lymphatics during inflammation[10]suggesting a role for NF-κB in regulation of VEGFR-3 expression. In the work supported by this proposal we have identified one of the central molecular mechanisms underlying inflammation- and tumor-induced lymphangiogenesis. Our current data, based on *in vivo* and *in vitro* models of inflammation, suggest that Prox1 and VEGFR-3 are directly regulated by inflammation through NF-κB signaling. These important and novel findings have set the basis for future studies that will investigate the primary functions of these factors in promoting breast cancer lymphatic metastasis.

Body

Task 1. To determine the synergistic effects of inflammatory mediators (TNF-α, IL-1β, and IL-6) on proliferation, migration and survival of lymphatic endothelial cells (LEC) induced by VEGFR-3 ligands in vitro. To accomplish this task, we will:

A. Measure effect of lymphangiogenic factors VEGF-C (50ng/ml) or VEGF-D (50ng/ml) on induction of LEC proliferation in the presence or absence of TNF-α (10ng/ml), IL-1β (10ng/ml), or IL-6 (10ng/ml).
B. Measure effect of lymphangiogenic factors VEGF-C (50ng/ml) or VEGF-D (50ng/ml) on LEC migration in the presence or absence of TNF-α (10ng/ml), IL-1β (10ng/ml), or IL-6 (10ng/ml).
C. Measure effect of lymphangiogenic factors VEGF-C (50ng/ml) or VEGF-D (50ng/ml) on LEC survival in the presence or absence of TNF-α (10ng/ml), IL-1β (10ng/ml), or IL-6 (10ng/ml).

Data toward accomplishment of Task 1:

In this report we have accomplished the following preliminary studies necessary for completion of the goals outlined in Task 1:

- cloned and characterized the human VEGFR-3 promoter
- demonstrated that NF-κB subunits p50 and p65 directly activate the VEGFR-3 promoter
- showed that NF-κB dependent inflammatory stimuli, IL-3 and LPS, upregulate endogenous VEGFR-3 expression in cultured LECs
- demonstrated that IL-3 and LPS induce LEC proliferation and migration
- showed that pretreatment with IL-3 and LPS enhances LEC proliferation and migration that is induced by the VEGFR-3 specific ligand, VEGF-C152S
- determined that NF-κB signaling is necessary for endogenous VEGFR-3 gene expression in LECs using sequence-specific and pharmacological NF-κB inhibitors
- demonstrated that primary mediators of lymphangiogenesis, Prox1 and VEGFR-3, are elevated during inflammatory lymphangiogenesis *in vivo*
- characterized the expression of inflammatory and lymphangiogenic mediators using a time-course mouse model of inflammation

- investigated whether VEGFR-3 upregulation is necessary for inflammation-induced angiogenesis.

Collectively, we have found that inflammation-induced NF-κB signaling directly activates the VEGFR-3 promoter. We hypothesize that this, in turn, increases VEGFR-3 receptor density that leads to greater activation by VEGFR-3 ligands, VEGF-C and VEGF-D, resulting in a more robust lymphangiogenic response. Results and methods relating to task completion of Task 1 is provided in the peer reviewed journal article entitled "Inflammation induces lymphangiogenesis through up-regulation of VEGFR-3 mediated by NF-kappaB and Prox1" (*Blood*. 2010 Jan 14;115(2):418-29) attached in appendix A of this report.

Task 2. To determine the effect of deficient NF-κB signaling on VEGFR-3 expression, lymphangiogenesis and tumor metastasis in an orthotopic breast cancer model in female p50 knockout mice. To accomplish this task, we will:

A. Implant syngeneic breast carcinoma cell lines (one non-metastatic and one highly metastatic derivative sub-line) in the MFP of wild-type (WT) and NF-κB p50 knockout mice (KO).
B. Assess the rate of tumor growth of breast cancer cell lines, tumor lymphangiogenesis, and lymphatic and distant metastasis.

Data toward accomplishment of Task 2

In this report we have accomplished the following preliminary studies necessary for completion of the goals outlined in Task 2A:

- Characterization of the lymphatic vessel density in the normal mammary fat pad (MFP) and other normal organs of adult female p50 KO and WT mice
- Characterization of expression of pro-lymphangiogenic proteins (e.g., VEGFR-3 and Prox1) in p50 KO and WT mice

In preparation of testing the effects of p50 KO on tumor growth and metastasis, we first characterized the lymphatic phenotype in the MFP and other normal organs of p50 KO and WT mice. In brief summary, these data showed that lymphatic vessel density (LVD) is significantly decreased in the lungs and liver of p50 KO mice, which corresponded to 25-44% decrease in VEGFR-3 and Prox1 expression. In the mammary fat pad (MFP), we found that despite a significant 20% decrease in LVD, expression of VEGFR-3 and Prox1 was

paradoxically elevated; demonstrating that the function of NF-κB p50 may be compensated for by other factors. This was supported by the fact that two other NF-κB subunits, p65 and p52, as well as ~35 inflammatory cytokines were elevated in the MFPs of p50 KO mice compared with WT. Collectively, these findings provide molecular insights into the key mechanism regulating postnatal lymphatic vessel formation, a critical process to both normal regulation of inflammatory response and pathological spread of lymphatic metastasis. Detailed methods for this section are reported in **appendix A.** Below I report in more detail these findings:

LYVE-1$^+$ vessel density is decreased in lung, liver and MFP of p50 KO mice

NF-κB dependent induction of inflammatory lymphangiogenesis has been shown in several animal models[28-31] including evidence obtained in our lab derived from a TG-induced peritonitis mouse model[32]. However, the specific role of the two major NF-κB proteins, p65 and p50, in postnatal formation and maintenance of normal lymphatic vessels has not been yet examined. The role of p65 is exceedingly difficult to examine postnatally due to embryonic lethality of this genotype[33]. In contrast, p50 KO mice survive to adulthood[34] and present an excellent *in vivo* model to clarify the role of NF-κB p50 in mechanisms controlling postnatal lymphangiogenesis in normal organs.

We previously showed that p50 is a direct transcriptional activator of the VEGFR-3 promoter in cultured LEC and that phosphorylation of p50 precedes both up-regulation of VEGFR-3 and the formation of new lymphatic vessels *in vivo*. Based on these findings, we hypothesized that p50 plays an important role in postnatal lymphangiogenesis and the absence of p50 would have a negative effect on lymphatic vessel formation in normal organs. To test this hypothesis, we determined LVD in seven major normal organs (lung, liver, MFP, kidney, heart, ovary and brain) of adult female p50 KO and WT mice by enumerating LYVE-1$^+$ vessels. As previously reported[35], the brain tissue had no lymphatic vessels in either p50 KO or WT mice. In the other six tissues with detectable LYVE$^+$ vasculature, LVD was significantly decreased in three organs of p50 KO mice as compared with WT. Table 2 shows the significant differences detected in: the lung (WT, 966 $\pm$ 90 vs. KO, 585 $\pm$ 55, $P < 0.001$); the liver (WT, 1307 $\pm$ 120 vs. KO, 1133 $\pm$ 83, $P = 0.05$); and the MFP (WT, 1917 $\pm$ 167 vs. KO, 1569 $\pm$ 144, $P < 0.001$). In contrast, kidney, heart, and ovary of p50 KO mice showed no significant changes compared with WT (Table 2). This suggested that NF-κB p50 might be essential for

postnatal lymphangiogenesis in the lung, liver, and MFP but dispensable in other organs due to possible compensation by other NF-κB transcription factors.

Decreased Decreased LVD correlates with suppressed VEGFR-3 and Prox1 expression in the lungs of p50 KO mice

The most conspicuous decrease in LVD in p50 KO mice was in the lung tissues (~40%, Table 2). Because VEGFR-3 and Prox1 are central mediators of lymphangiogenesis[36;37] and their expression has been shown to be regulated by NF-κB p50 [38], we hypothesized that decreased pulmonary LVD might be mediated by deficient expression of VEGFR-3 or Prox1. To test this hypothesis, we compared mRNA levels of LYVE-1 with those of VEGFR-3 and Prox1. The results showed that expression levels of all three lymphatic markers (i.e., LYVE-1, VEGFR-3, and Prox1) were significantly reduced in the lungs of p50 KO mice compared with WT (Table 2). LYVE-1 transcripts were decreased by 32 ± 4% (P = 0.03), whereas VEGFR-3 and Prox1 were reduced by 25 ± 10% (P = 0.17) and 44 ± 4% (P = 0.04), respectively (Table 3). This finding suggests that p50 NF-κB regulates VEGFR-3 and Prox1 expression in lung lymphatic vessels and that the absence of p50 suppresses the formation of pulmonary lymphatic vasculature.

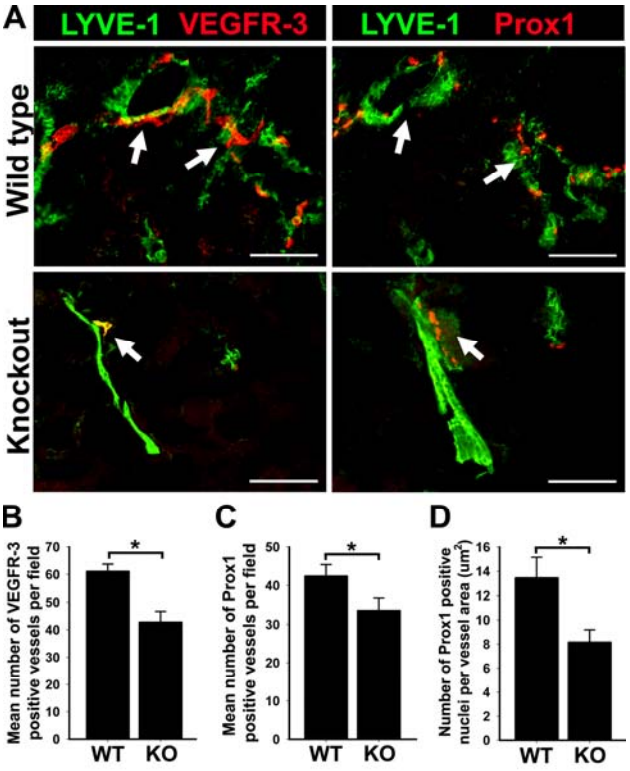

Figure 1. Decreased lymphatic vessel density and reduced expression of Prox1 and VEGFR-3 in the lungs of p50 KO mice compared with WT. (**A**) Double immunoflourescent staining with anti-LYVE-1 and anti-VEGFR-3 or anti-Prox1 antibodies in serial sections of p50 KO and WT lungs, showing reduced lymphatic vessel density. Arrows indicate overlapping expression of VEGFR-3 and Prox1 on LYVE-1$^+$ lymphatic vessels on serial sections of p50 KO and WT lungs. Scale bar represents 100 μm. Mean lymphatic vessel density of VEGFR-3 (**B**) and Prox1 (**C**) positive vessels was measured from 3 images of p50 KO and WT lungs (n = 5 mice per group) acquired at 200X magnification. Data are presented as the mean vascular area ± SEM. The P values represent *<0.05 and **<0.01 as determined by Student's unpaired t-test. (**D**) The number of Prox1 positive nuclei were enumerated in 5 images of p50 KO and WT lungs (n = 3-4 mice per group) acquired at 200X magnification. Density of Prox1 positive nuclei was normalized per LYVE-1 positive lymphatic vessel area (μm^2) and is presented as the average number of Prox1 positive nuclei per vessel area ± SEM. The P value represents *<0.05 as determined by Student's unpaired t-test.

To determine whether the levels of VEGFR-3 and Prox1 proteins normalized per LYVE-1$^+$ vessel area are also reduced (i.e., relative expression per lymphatic vessel), we calculated the relative MFI in individual lymphatic vessels (described in the Methods). The MFI

values did not differ significantly between WT and KO suggesting that the observed reduction in VEGFR-3 and Prox1 expression levels (Table 3) is due to decreased density of positive vessels rather than to altered protein expression level in individual vessels. To clarify this point, we enumerated VEGFR-3$^+$ and Prox1$^+$ lymphatic vessels and normalized these values per tissue area. This analysis showed a significantly decreased density of VEGFR-3$^+$ and Prox1$^+$ lymphatic vessels by 30% (P = 0.03) and 20% (P = 0.04), respectively (Figure 1B, C). Moreover, when Prox1$^+$ nuclei were enumerated and normalized per LYVE-1$^+$ vessel area, the decrease in Prox1$^+$ nuclei in p50 KO mice reached 40% (P = 0.01) compared with p50 WT mice (Figure 1D). Collectively, these findings suggest that NF-κB p50 is directly responsible for regulation of the key lymphangiogenic proteins, VEGFR-3 and Prox1, in postnatal pulmonary lymphatic vessels.

Decreased LVD correlates with reduced expression of VEGFR-3 in the liver of p50 KO mice

LYVE-1$^+$ vessel density in the liver of p50 KO mice was also significantly reduced by 13.4% (P = 0.05) as compared with WT mice (Table 2). The reduction in LVD corresponded to a 44% decrease in LYVE-1 transcripts (P = 0.02) determined by qRT-PCR (data not shown). In line with decreased LYVE-1 expression, VEGFR-3 mRNA was also reduced by 29 ± 6% (P = 0.004, Table 3). The reduction in VEGFR-3 mRNA levels also corresponded to decreased expression of VEGFR-3 protein as determined by MFI analysis of slides double-stained with anti-VEGFR-3 and anti-LYVE-1 antibodies (Figure 2). These data indicate that the absence of p50 in the liver causes a coordinated decrease of LYVE-1$^+$ vessels and

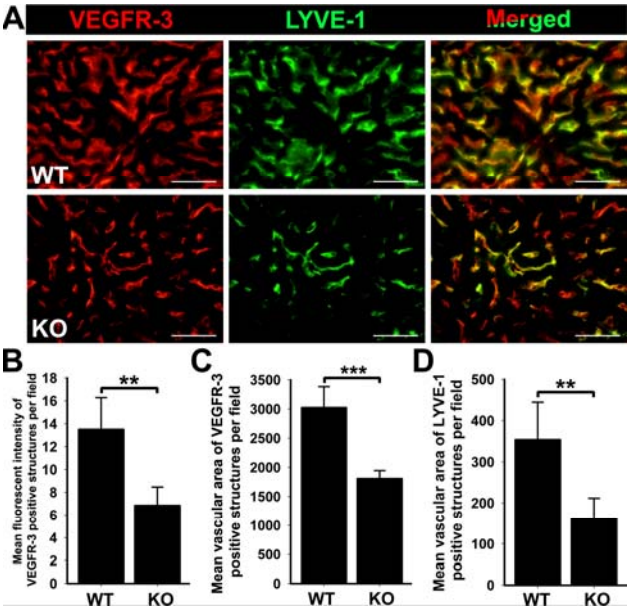

Figure 2. Deletion of NF-κB p50 KO results in decreased expression of VEGFR-3 and LYVE-1 on liver endothelial cells compared with WT. (**A**) Livers of p50 KO and WT mice were double immunostained with anti-VEGFR-3 and anti-LYVE-1 antibodies, showing decreased VEGFR-3 expression in endothelial cells of p50 KO livers compared with WT. Scale bars represent 50 μm. (**B**) The mean fluorescent intensity of VEGFR-3 staining was analyzed in 3 random fields of p50 KO and WT livers (n = 5 mice per group) at 400X magnification. Data are presented as the mean fluorescent intensity ± SEM. The P value represents **<0.01 as determined by Student's unpaired t-test. The mean vascular area of VEGFR-3 (**C**) and LYVE-1 (**D**) positive staining was calculated from 3 independent images of p50 KO and WT livers (n = 5 mice per group). Data are presented as the mean vascular area normalized per total area ± SEM. The P values represent **<0.01 and ***<0.001 as determined by Student's unpaired t-test.

VEGFR-3 expressed on these vessels.

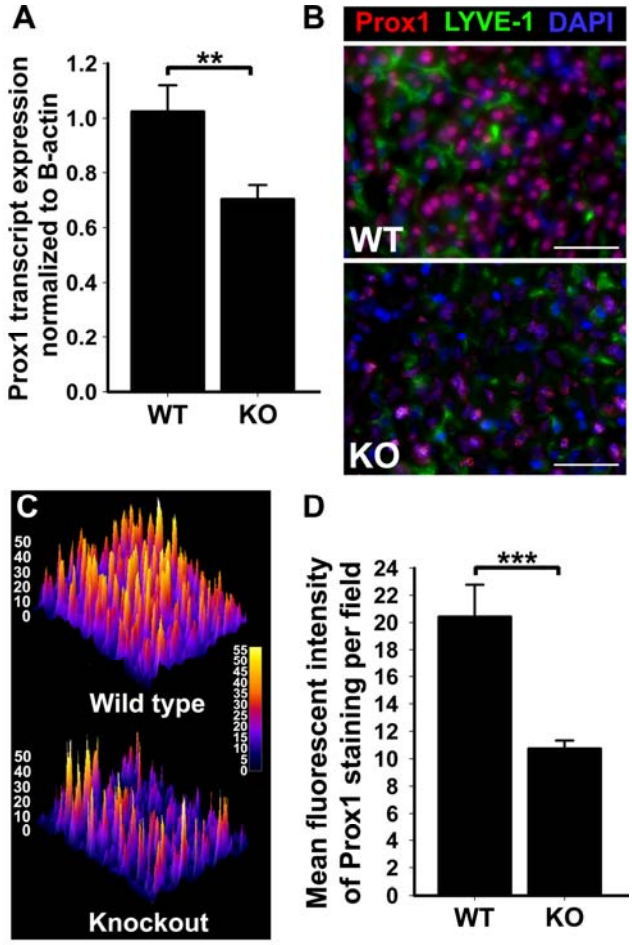

Figure 3. Expression of Prox1 in the mouse liver is significantly decreased by deletion of NF-κB p50 KO as compared with WT. (**A**) Quantitative RT-PCR analysis of Prox1 transcript expression in total RNA extracted from p50 KO and WT livers (n = 5 mice per group). Relative expression was normalized to β-actin. Data are presented as mean transcript expression ± SEM. *P* values are indicated as *<0.01 as determined by Student's unpaired t-test. (**B**) Liver sections were double immunostained with anti-Prox1 and anti-LYVE-1 antibodies. Scale bars represent 50 μm. (**C**) A representative surface plot of the fluorescent intensity of Prox1 staining in p50 KO and WT liver sections. Note in panels (**B**) and (**C**) a dramatic reduction in Prox1 expression in both liver sinusoidal endothelial cells and hepatocytes. (**D**) The mean fluorescent intensity of Prox1 staining was analyzed in 3 random fields of p50 KO and WT livers (n = 5 mice per group) acquired at 400X magnification. Data are presented as the mean fluorescent intensity ± SEM. The *P* value represents ***<0.001 as determined by Student's unpaired t-test.

As previously reported, both lymphatic and blood hepatic sinusoidal endothelial cells express LYVE-1 and VEGFR-3 [35;39]. In p50 KO mice, VEGFR-3 protein significantly decreased by 51 ± 12% in both types of vascular cells compared with corresponding cells in WT mice (*P* = 0.002, Figure 2B and Table 3). Another perturbed vascular parameter in p50 KO livers was marked reduction in the total area of VEGFR-3$^+$ and LYVE-1$^+$ sinusoidal endothelium (Figure 2A). A similar phenotype has been demonstrated in *Tie2-Cre/IKKβ* mice with targeted disruption of canonical NF-κB p50 and p65 signaling in the endothelial cell compartment[40]. This report and our prior findings in cultured LECs suggested that NF-κB p50-mediated expression of VEGFR-3 might be important for the formation of the endothelium-lined hepatic sinusoids. To confirm this hypothesis, we quantified the mean vascular area of VEGFR-3$^+$/LYVE-1$^+$ vessels on images acquired from p50 KO and WT liver sections using Image J software. Compared with WT, the mean vascular area of VEGFR-3$^+$ and LYVE-1$^+$ vessels in p50 KO livers was significantly decreased by 40% and 55%, respectively (Figure 2C, D). Collectively, these findings demonstrate that the NF-κB p50-mediated VEGFR-3 expression in the liver may contribute to the optimal density of both blood and lymphatic vasculature.

Expression of Prox1 is decreased in both liver endothelial cells and hepatocytes of p50 KO mice

We previously reported that lymphatic expression of Prox1 is drastically increased in an inflammatory setting, presumably due to activation of the NF-κB pathway in the lymphatic endothelium[38]. However, the mechanisms regulating Prox1 expression under normal physiological conditions are presently unknown. Based on our prior findings[38], we postulated that NF-κB p50 might be required for postnatal regulation of Prox1 expression in normal organs. The liver is an interesting organ to test this hypothesis because in this tissue Prox1 is expressed in both lymphatic endothelial cells and hepatocytes[41]. We, therefore, analyzed livers from p50 KO and WT mice for Prox1 mRNA and protein by qRT-PCR and immunofluorescent staining, respectively (Figure 3). As compared with WT mice, expression of both Prox1 mRNA and protein were reduced by ~30% (Figure 3A, B and Table 3) with differences being statistically significant (P = 0.03). Reduction in Prox1 protein was observed in both hepatocytes and LYVE-1$^+$ endothelial cells (Figure 3B). Protein levels of Prox1 were also analyzed through comparison of MFI from Prox1-immunofluorescent staining of p50 KO and WT liver sections. This analysis also showed a highly significant (P < 0.001) decrease of 47 ± 3% in p50 KO liver cells as compared with WT counterparts (Figure 3C, D and Table 3). These findings indicate that in the context of liver tissue, NF-κB p50 has a significant impact on Prox1 expression in both endothelial and non-endothelial cell types.

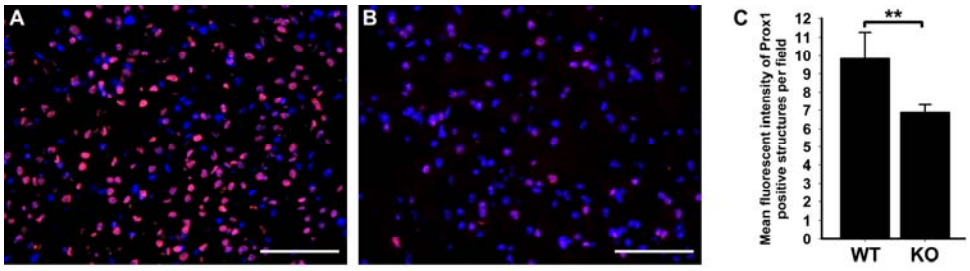

Figure 4. Cell-type specific downregulation of Prox1 in neurons of p50 KO brains compared with WT. Frozen sections of p50 WT (**A**) and KO (**B**) brains were immunostained with anti-Prox1 antibodies and counterstained with DAPI. Note the dramatic reduction in the fluorescent intensity of Prox1 immunostaining in p50 KO compared with WT. (**C**) Analysis of the MFI of Prox1 staining in p50 KO and WT neurons (n = 3-4 mice per group). Data are presented as MFI of Prox1 staining ± SEM. The P value represents **<0.01 as determined by Student's unpaired t-test.

Expression of Prox1 is decreased in the brain, but not in the heart, of p50 KO mice

In addition to hepatocytes, Prox1 has also been detected in several other non-lymphatic endothelial cell types including cardiomyocytes[42] and neurons[43]. We, therefore, sought to determine whether the absence of p50 in brains and hearts of p50 KO mice causes similar decrease in Prox1 expression as observed in the liver. To answer this question, Prox1 expression was analyzed on mRNA and

protein levels using qRT-PCR and MFI, respectively. In the brain of p50 KO mice, transcripts and protein levels of Prox1 were reduced by 51 ± 12% and 25 ± 3%, respectively, compared with WT (Figure 4A-C and Table 3), with both values being statistically significant (*P* = 0.01, Table 3). In contrast, no change in Prox1 expression was observed in the heart of p50 KO (data not shown), suggesting that the regulatory effect of p50 NF-κB on Prox1 expression might be tissue-specific, being prominent in some organs but dispensable in others.

The MFPs of p50 KO mice exhibit decreased LYVE-1$^+$ LVD but aberrantly increased VEGFR-3 and Prox1 expression on lymphatic vasculature

The mouse mammary fat pad (MFP) is a tissue with very high LVD, which prompted us to investigate the effects of p50 deletion on postnatal lymphatic formation and expression of lymphatic-specific proteins. We first compared anti-LYVE-1 antibody stained MFPs from p50 KO and WT mice (Figure 5A). This analysis revealed a ~20% decrease in density of LYVE-1$^+$ vessels (*P* <0.001, Table 2 and Figure 5B) and ~60% decrease in mean vascular area of LYVE-1$^+$

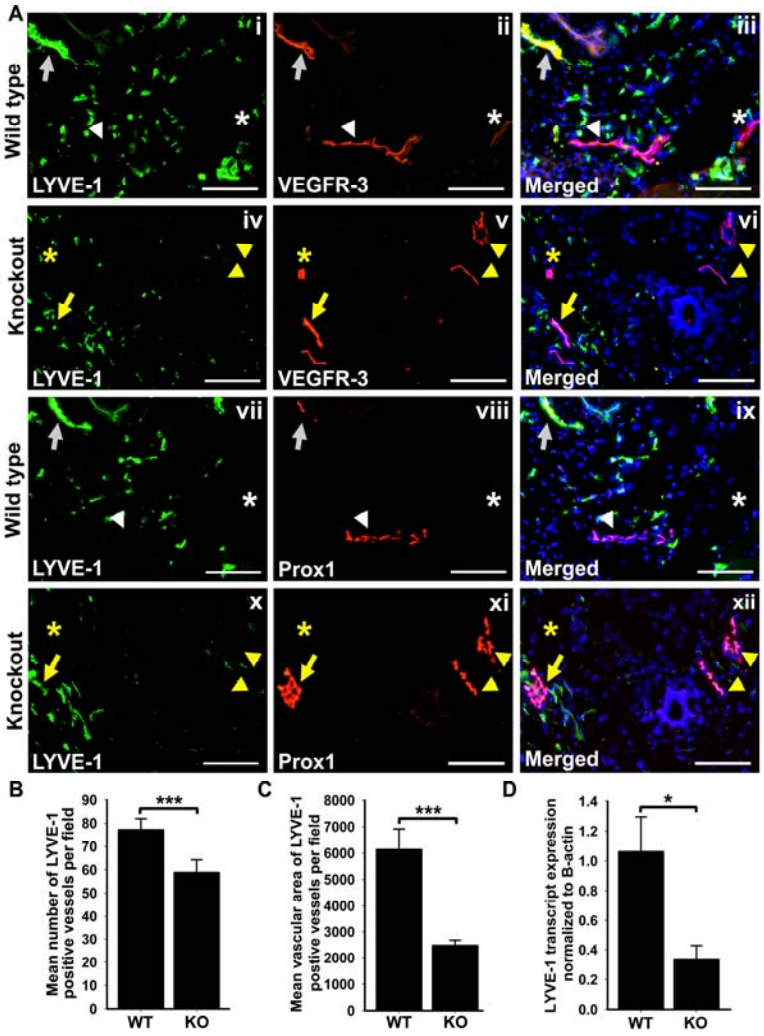

Figure 5. Decreased LYVE-1$^+$ lymphatic vessel density despite elevated expression of VEGFR-3 and Prox1 in the MFP of p50 KO mice compared with WT. (**A**) Serial frozen sections of p50 KO and WT MFP were double-immunostained with anti-LYVE-1 and anti-VEGFR-3 (i-vi) or anti-LYVE-1 and anti-Prox1 (vii-xi) antibodies. Scale bar represents 100 μm. Some VEGFR-3$^+$/Prox1$^+$ lymphatic vessels also expressed LYVE-1 (arrows), whereas other VEGFR-3$^+$/Prox1$^+$ lymphatic vessels were LYVE-1 negative (arrowhead). Vascular structures resembling blood vessels also stained positive for VEGFR-3 but negative for lymphatic markers Prox1 and LYVE-1 (asterisk). Note that overall density and expression of VEGFR-3$^+$/Prox1$^+$ was increased in p50 KO (iv-vi and x-xii) compared with WT (i-iii and vii-ix). (**B**) LYVE-1 positive lymphatic vessels were enumerated in 6 images per p50 KO and WT MFPs (n = 3 mice per group) acquired at 200X magnification. The results are presented as the mean LYVE-1 positive vessel density per 200X field ± SEM. The *P* value represents ***<0.001 as determined by Student's unpaired t-test. (**C**) The mean vascular area of LYVE-1 positive vessels was measured from 3 images of p50 KO and WT MFPs (n = 3 mice per group) acquired at 200X magnification. The *P* value represents ***<0.001 as determined by Student's unpaired t-test. (**D**) Quantitative RT-PCR analysis of LYVE-1 was performed using total RNA extracted from p50 KO and WT MFPs (n = 4-5 mice per group). Relative expression was normalized to β-actin. Data are presented as the mean β-actin normalized transcript expression ± SEM. The *P* value represents *<0.05 as determined by Student's unpaired t-test.

staining per section area in p50 KO mice (P <0.001, Figure 5C). This finding was corroborated by qRT-PCR analysis that detected a corresponding 66 ± 9% decrease in LYVE-1 transcripts (P = 0.01, Figure 5D). Surprisingly, however, the number of VEGFR-3$^+$ and Prox1$^+$ lymphatic vessels was slightly higher in p50 KO mice compared with WT, although the differences did not reach statistical significance (data not shown). Additionally, the MFI of VEGFR-3 and Prox1 in lymphatic vessels was elevated by 134 ± 12% (P = 0.001) and 123 ± 15% (P = 0.05), respectively, in p50 KO mice compared with WT (Table 3). This was corroborated by statistically significant 1.8-fold and 2.4-fold increases in VEGFR-3 and Prox1 transcripts, respectively, as detected by qRT-PCR (Table 3). These findings indicated that although the density of LYVE-1$^+$ vessels was reduced in the MFPs of p50 KO mice, the expression levels of VEGFR-3 and Prox1 per vessel were significantly increased. These findings suggested that in the MFP context, p50 ablation is associated with deficient formation of lymphatic vessels despite causing overexpression of some lymphatic markers, through possibly alternative transcriptional mechanisms.

Weak expression of VEGFR-3 on normal MFP blood vasculature is not affected by p50 deletion

VEGFR-3 has also been reported to be weakly expressed on blood vessels of normal breast tissue and elevated on the angiogenic blood vessels in breast tumors[44] and other malignant tissues[45;46]. We, therefore, investigated whether lack of NF-κB p50 might also affect VEGFR-3 expression on blood vasculature in the MFP of p50 KO and WT mice, using antibodies against VEGFR-3 and a blood vascular-specific marker, MECA-32[47]. MFP blood vessels in both p50 KO and WT mice were uniformly stained with anti-MECA-32 antibody (Figure 6). Weak expression of VEGFR-3 was detected on subsets of MECA-32$^+$ blood vessels without appreciable differences between p50 KO and WT mice (Figure 6) suggesting that, in contrast to lymphatic endothelium, blood vascular expression of VEGFR-3 is not affected by lack of p50. To confirm this conclusion, we examined the blood-specific VEGFR-3 expression in two organs previously

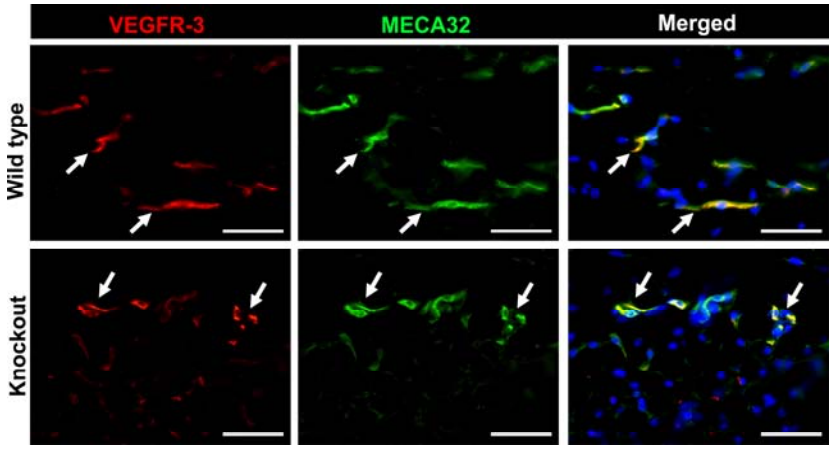

Figure 6. VEGFR-3 expression on quiescent MFP blood vessels is unchanged by deletion of NF-κB p50. Frozen sections of p50 KO and WT MFP were immunostained with anti-VEGFR-3 and anti-MECA32 antibodies. Scale bare represents 50 μm. Arrows indicate overlapping expression of VEGFR-3 and MECA32 in MFP blood vessels.

reported to express VEGFR-3 on blood vessels: the kidney[35] and the ovary[46]. This analysis also revealed no changes in the blood vascular-specific expression of VEGFR-3 (data not shown), suggesting that its expression on blood vasculature is regulated in a p50-independent manner.

Elevated VEGFR-3 and Prox1 expression on lymphatic vasculature of the MFPs of p50 KO mice is associated with inherent inflammation

To explain the paradoxical increase of VEGFR-3 and Prox1 in MFP lymphatic vessels, we hypothesized that the absence of p50 in this tissue is compensated by other members of the NF-κB family whose pro-inflammatory signaling up-regulates VEGFR-3 and Prox1 expression but is insufficient for generation of new lymphatic vessels. This is plausible because NF-κB subunits p65 and p52 have been previously reported to compensate for the lack of p50[48]. To determine whether these subunits could be differentially expressed in tissues of p50 KO and WT mice, we analyzed p65 and p52 expression levels by qRT-PCR. This analysis revealed a nearly perfect correlation between changes in expression levels of VEGFR-3 and NF-κB p65 in each organ examined (Table 4). For example, both VEGFR-3 and p65 were reduced in lung and liver, elevated in MFP, and close to level of WT mice in kidney, heart, and brain. Similarly, the pattern of NF-κB p52 expression was highly correlative with Prox1 profile, with both genes being reduced in lung, liver and brain, elevated in MFP, and roughly unchanged in kidney and heart (Table 4). These data suggested that in the absence of p50 VEGFR-3 and Prox1 expression might be regulated by p65 and p52 NF-κB subunits overexpressed in the MFP of p50 KO mice.

Positive correlation between expression levels of VEGFR-3 and Prox1 and p65/p52 NF-κB subunits suggested that the MFP tissue compensates for the lack of p50 by up-regulating both canonical (p65) and non-canonical (p52) NF-κB pathways. This finding suggested that overexpression of p50-alternative transcription factors might create a pro-inflammatory rather than an anti-inflammatory environment. To test this hypothesis, we compared the expression levels of 84 NF-κB-dependent genes in the MFP of p50 KO and WT mice by using an inflammation gene-targeted PCR array. We found that a large portion of the tested genes (35 of 84, or 41.6% of total) expressed in the MFP of p50 KO mice were elevated by at least 1.5-fold compared with the MFP gene profile in WT mice (Table 5). A smaller fraction (28.5%) was down-regulated in p50 KO MFPs by at least 1.5-fold, while the level of remaining genes was unchanged. This finding suggested

that VEGFR-3 and Prox1 are upregulated in MFPs of NF-κB p50 KO mice due to aberrant inflammation induced by compensatory over-expression of two factors of the NF-κB family, p65 and p52. However, the pathways induced by these two transcription factors were insufficient for maintaining normal level of postnatal lymphangiogenesis mediated by p50 subunit as indicated by the 18% reduction in LVD in MFPs of p50 KO mice as compared with WT (Table 2). This evidence further underscores the essential role of the NF-κB p50 subunit in postnatal formation of lymphatic vessels in normal tissues.

Table 1. Lymphatic vessel density (LVD) in normal organs of p50 KO and WT mice

	LVD (per mm^2)[†]			
Organ	WT	KO	Percent decrease	*P*-value
Lung	966 ± 90	585 ± 55[*]	39.4%	<0.001
Liver	1307 ± 120	1133 ± 83	13.4%	0.05
MFP	1917 ± 167	1569 ± 144	18.2%	<0.001
Kidney	11 ± 3	11 ± 2[#]	0.0%	n.s.[‡]
Heart	125 ± 9	126 ± 10	0.0%	n.s.
Ovary	1049 ± 104	938 ± 184	10.6%	n.s.
Brain	No LV detected		—	—

[†]LVD was calculated from frozen organ sections stained with anti-LYVE-1 antibodies. Three independent images were acquired per animal (n = 3-5 mice per group). Data are presented as mean LVD ± SEM.

[#]LVD was normalized to the tissue circumference

[‡]n.s. denotes non-significant changes

Table 2. Relative changes in Prox1 and VEGFR-3 expression in normal organs of p50 KO versus WT mice

	Prox1				VEGFR-3			
Organ	qRT-PCR[¶]	*P*-value	MFI[‡]	*P*-value	qRT-PCR[¶]	*P*-value	MFI[‡]	*P*-value
Lung	56 ± 4%	0.04[*]	104 ± 5%	n.s.[‡]	75 ± 10%	n.s.	99 ± 19%	n.s.
Liver	70 ± 5%	0.03	53 ± 3%	<0.001	71 ± 6%	0.004	49 ± 12%	0.002
MFP	243 ± 45%	0.02	123 ± 15	0.05	180 ± 29%	0.05	134 ± 12%	0.001
Kidney	90 ± 13%	n.s.	100 ± 9%	n.s.	85 ± 6%	n.s.	100 ± 8%	n.s.
Heart	82 ± 15%	n.s.	98 ± 1%	n.s.	96 ± 6%	n.s.	103 ± 6%	n.s.
Ovary	103 ± 27%	n.s.	85 ± 5%	0.004	126 ± 42%	n.s.	102 ± 9%	n.s.
Brain	49 ± 12%	0.01	75 ± 3%	0.01	109 ± 8%	n.s.	—	—

[¶] Transcript expression analyzed by qRT-PCR and presented as the percent expression in p50 knockouts compared with wild type control mice (n = 3-5 mice per group)

[‡] Mean fluorescent intensity (MFI) presented as the percent expression in p50 knockouts compared with wild type control mice (n = 3-5 mice per group)

[*]P value was determined by Student's unpaired t-test

[‡]denotes non-significant changes

Table 3. Comparison of Prox1 and VEGFR-3 transcripts to expression of NF-κB p65 and p52 subunits in p50 KO vs. WT mice

Tissue[†]	*Prox1*	*VEGFR-3*	*p65 (Rela)*	*P*	*p52 (NF-κB2)*	*P*
Lung	56 ± 4%	75 ± 10%	58 ± 5%	<0.001	57 ± 10%	0.05
Liver	70 ± 5%	71 ± 6%	79 ± 2%	0.002[‡]	76 ± 5%	0.05
MFP	243 ± 45%	180 ± 29%	140 ± 4%	0.001	158 ± 2%	0.005
Kidney	90 ± 13%	85 ± 6%	100 ± 6%	n.s.[¶]	88 ± 10%	n.s.
Heart	82 ± 15%	96 ± 6%	90 ± 3%	0.03	69 ± 2%	<0.001
Brain	49 ± 12%	109 ± 8%	97 ± 7%	ns	76 ± 5%	0.03

[†] cDNA synthesized from total RNA extracted from each tissue (n = 3-5 mice per group)

[‡] P value was determined by Student's unpaired t-test

[¶] denotes non-significant changes

Table 4. Changes in expression of inflammatory mediators in MFPs of p50 KO vs. WT mice

Gene name	Symbol	Fold change compared with WT	Gene name	Symbol	Fold change compared with WT
Interleukin 17B[¶]	Il17b	9.25[‡]	Chemokine (C-C motif) ligand 20	Ccl20	1.16
Complement component 3	C3	6.06	Interleukin 4	Il4	1.16
Chemokine (C-C motif) receptor 10	Ccr10	5.86	Interleukin 16	Il16	1.14
Tumor necrosis factor receptor superfamily, member 1a	Tnfrsf1a	4.72	Chemokine (C-C motif) ligand 17	Ccl17	1.12
			Interferon gamma	Ifng	1.10
Macrophage migration inhibitory factor	Mif	3.89	Chemokine (C-C motif) ligand 24	Ccl24	1.10
Interleukin 13 receptor, alpha 1	Il13ra1	3.61	Chemokine (C-C motif) receptor 9	Ccr9	1.09
Small inducible cytokine subfamily E, member 1	Scye1	3.27	Interleukin 1 alpha	Il1a	1.07
			Chemokine (C-C motif) ligand 19	Ccl19	1.06
Interleukin 6 signal transducer	Il6st	3.12	Chemokine (C-C motif) receptor 4	Ccr4	1.06
Interleukin 18	Il18	2.83	Chemokine (C-X-C motif) ligand 5	Cxcl5	1.06
ATP-binding cassette, sub-family F (GCN20), member 1	Abcf1	2.73	Chemokine (C-C motif) ligand 3	Ccl3	1.01
			Interleukin 1 receptor, type II	Il1r2	1.00
Chemokine (C-X-C motif) ligand 15	Cxcl15	2.68	Chemokine (C-C motif) receptor 2	Ccr2	0.93
Chemokine (C-C motif) ligand 11	Ccl11	2.62	Chemokine (C-C motif) ligand 6	Ccl6	0.90
B-cell leukemia/lymphoma 6	Bcl6	2.60	Chemokine (C-C motif) ligand 9	Ccl9	0.88
Chemokine (C-X3-C motif) ligand 1	Cx3cl1	2.60	Interleukin 10 receptor, alpha	Il10ra	0.87
Chemokine (C-C motif) receptor 5	Cxcr5	2.51	Chemokine (C-C motif) ligand 7	Ccl7	0.84
C-reactive protein, pentraxin-related	Crp	2.50	Integrin alpha M	Itgam	0.81
Chemokine (C-X-C motif) ligand 12	Cxcl12	2.28	Chemokine (C-C motif) ligand 2	Ccl2	0.77
Interleukin 15	Il15	2.27	Interleukin 1 beta	Il1b	0.76
Secreted phosphoprotein 1	Spp1	2.17	Chemokine (C-C motif) ligand 4	Ccl4	0.69
Interleukin 1 receptor, type I	Il1r1	1.93	Chemokine (C-C motif) ligand 12	Ccl12	0.66
Interleukin 1 family, member 8	Il1f8	1.85	Chemokine (C motif) receptor 1	Xcr1	0.64
Chemokine (C-C motif) receptor 1	Ccr1	1.80	Integrin beta 2	Itgb2	0.62
Chemokine (C-X-C motif) ligand 9	Cxcl9	1.74	Interleukin 5 receptor, alpha	Il5ra	0.60
Interleukin 11	Il11	1.74	Chemokine (C-C motif) ligand 1	Ccl1	0.59
Transforming growth factor, beta 1	Tgfb1	1.74	Chemokine (C-X-C motif) ligand 1	Cxcl1	0.59
Chemokine (C-X-C motif) ligand 10	Cxcl10	1.71	Interleukin 8 receptor, beta	Il8rb	0.59
Chemokine (C-X-C motif) ligand 11	Cxcl11	1.69	Interleukin 10	Il10	0.48
Interleukin 6 receptor, alpha	Il6ra	1.69	Chemokine (C-X-C motif) receptor 3	Cxcr3	0.45
Toll interacting protein	Tollip	1.69	Interleukin 3	Il3	0.39
Caspase 1	Casp1	1.68	Interleukin 2 receptor, beta chain	Il2rb	0.37
Tumor necrosis factor receptor superfamily, member 1b	Tnfrsf1b	1.65	Chemokine (C-X-C motif) ligand 13	Cxcl13	0.36
			Chemokine (C-C motif) receptor 8	Ccr8	0.28
Platelet factor 4	Pf4	1.61	Lymphotoxin A	Lta	0.24
Chemokine (C-C motif) ligand 8	Ccl8	1.59	Chemokine (C-C motif) receptor 7	Ccr7	0.24
Interleukin 10 receptor, beta	Il10rb	1.57	Interleukin 2 receptor, gamma chain	Il2rg	0.16
Chemokine (C-C motif) receptor 3	Ccr3	1.51	Chemokine (C-C motif) receptor 6	Ccr6	0.16
Tumor necrosis factor	Tnf	1.49	Chemokine (C-C motif) ligand 5	Ccl5	0.13
Chemokine (C-C motif) ligand 25	Ccl25	1.43	Chemochine (C-X-C motif) receptor 5	Ccr5	0.12
Interleukin 13	Il13	1.38	Lymphotoxin B	Ltb	0.07
Interleukin 20	Il20	1.27	CD40 ligand	Cd40lg	0.05
Interleukin 1 family, member 6	Il1f6	1.26	Chemokine (C-C motif) ligand 22	Ccl22	0.04

[‡] Fold changes were derived from qRT-PCR array analysis of total MFP mRNA from p50 KO and WT mice (n = 4 mice per group)

[¶] Gray shading indicates genes with greater than 0.5-fold change expression in p50 KO compared with WT MFP

Data from this section is currently under peer review at the journal *Microcirculation.* Work towards completion of Task 2A and 2B is scheduled for the next year. The analysis of this aim is likely to be completed in the third year of the proposal.

Task 3. To determine the effect of anti-inflammatory treatment on VEGFR-3 expression, tumor lymphangiogenesis, lymphatic metastasis, and spread to distant organs in an orthotopic model of human breast carcinoma, MDA-MB-231. To accomplish this task, we will:

A. Implant luciferase tagged human breast carcinoma line MDA-MB-231 into the MFP of CB-17 SCID mice and treat them with NF-κB targeting anti-inflammatory drugs, PDTC and dexamethasone.
B. Assess tumor growth, tumor lymphangiogenesis, and lymphatic metastasis to distant organs.

Execution of this aim is scheduled for the next year. The analysis of this aim is likely to be completed in the third year of the proposal.

Key research accomplishments

Year 2 Annual Report

- Cloned and characterized nine human VEGFR-3 promoter-reporter constructs ranging from -849bp to -46bp relative to the transcription start site
- Identified NF-κB subunits p50 and p65 as key regulators of the VEGFR-3 promoter *in vitro* by using ChIP and promoter-reporter analyses
- Identified the lymphatic-specific transcription factor, Prox1, as a direct activator of the VEGFR-3 promoter *in vitro* by using ChIP and promoter-reporter analyses
- Discovered using a time-course model of inflammatory lymphangiogenesis that expression of Prox1 is rapidly increased by 1-2 days after the onset of inflammation and this is followed a 3-fold in VEGFR-3 protein expression 2-3 days later
- Found that upregulation of both Prox1 and VEGFR-3 precedes inflammation-induced formation of new lymphatic vessels
- Determined that the NF-κB dependent inflammatory stimuli, IL-3 and LPS, increase VEGFR-3 transcript expression by 4- to 6-fold
- Showed that increased VEGFR-3 expression in response to inflammatory mediators increases LEC responsiveness of to VEGFR-3 specific ligands.
- Characterized lymphatic vessel density in p50 KO and WT mice
    - Showed that LVD in the liver, lungs, and MFP of KO mice was reduced by 40%, 14%, and 19%, respectively.
- Characterized expression of the primary pro-lymphangiogenic mediators, Prox1 and VEGFR-3, in p50 KO mice compared with WT.
    - Showed 25-44% decreased VEGFR-3 and Prox1 expression in lung and liver of p50 KO mice compared with WT, respectively.
    - Despite reduced LVD in the MFP of p50 KO mice, there was a paradoxical increase in VEGFR-3 and Prox1 expression by 80-140% compared with in WT.
    - Analysis of p65 and p52 NF-κB subunits and an array of inflammatory mediators showed a significant increase in p50 alternative pathways in the MFP but not other organs, suggesting

that compensatory mechanisms may regulate VEGFR-3 and Prox1 in the absence of NF-κB p50 in the MFP. However, the significantly reduced LVD in the MFP suggests that additional p50-dependent signals may be required for normal lymphangiogenesis.

Reportable outcomes

Year 2 Annual Report

Peer Reviewed Journal Articles

1. **Michael J. Flister**, Andrew Wilber, Kelly L. Hall, Caname Iwata, Kohei Miyazono, Riccardo E. Nisato, Michael S. Pepper, David C. Zawieja and Sophia Ran. Inflammation induces lymphangiogenesis through upregulation of VEGFR-3 mediated by NF-κB and Prox1. *Blood*. 2010 Jan 14;115(2):418-29. Epub 2009 Nov 9.
2. Sophia Ran, Lisa Volk, Kelly Hall, and **Michael J. Flister.** Lymphangiogenesis and Lymphatic Metastasis in Breast Cancer. *Pathophysiology*. 2009 Dec 23. [Epub ahead of print]

Awards/Presentations:

1. 2nd Place Presentation in 20th Annual Trainee Symposium, SIU School of Medicine, May 2010.
2. Bradley University Alumni Spotlight, March 2010
3. Selected to the U.S. Delegation for the 60th Meeting of Nobel Laureates in Lindau, Germany, June, 2010.
4. Best Student Publication Award for 2009.

Published Abstracts:

1. **Flister MJ,** Hall K, Wilber A, and Ran S. Inflammatory mediators activate lymphatic endothelial cells (LECs) through elevation of NF-κB, Prox1, and VEGFR-3. American Association for Cancer Research Annual Meeting, Washington DC, 2010.
2. Hall K, **Flister MJ**, Volk L, Curry S, Wilber A, and Ran S. Angiopoietin-2 role in breast cancer metastasis. American Association for Cancer Research Annual Meeting, Washington DC, 2010.

Conclusions:

Conclusions of work towards completion of Task 1:

Here we have presented the first molecular evidence that VEGFR-3, the central mediator of lymphangiogenesis, is directly regulated by NF-κB transcription factors, p50 and p65, in response to extracellular inflammatory stimuli. We also present novel evidence that the lymphatic-specific transcription factor Prox1 is induced by NF-κB-dependent inflammation and elevation of both NF-κB and Prox1 preceded upregulation of VEGFR-3 by 2-3 days *in vivo*. *In vitro* we demonstrated that NF-κB and Prox1 transcription factors directly transactivate the VEGFR-3 promoter. Moreover, our data show that NF-κB dependent mediators, IL-3 and LPS, increased Prox1 and VEGFR-3 expression and responsiveness of LECs to the VEGFR-3 specific ligand, VEGF-C152S. Collectively, these results suggest that LEC stimulation by NF-κB-dependent cytokines amplifies the lymphangiogenic signals by increasing VEGFR-3 expression.

Conclusions of work towards completion of Task 2:

This preliminary systematic comparison of VEGFR-3 and Prox1 expression in the lymphatics of normal organs in p50 KO and WT mice was important to lay the foundation for future experiments characterizing the effects of p50 deletion on breast cancer growth, lymphangiogenesis and lymphatic metastasis. During this analysis, we have made several novel observations that give broader implications to the functions of NF-κB, Prox1, and VEGFR-3 in normal vascular and non-vascular physiology. These include: 1) original evidence for the essential role of NF-κB p50 in organ-specific lymphatic development and expression of the key pro-lymphangiogenic proteins, VEGFR-3 and Prox1, under normal conditions; 2) strong associations among VEGFR-3, Prox1 and lymphatic vessel density that support the notion that NF-κB controls normal lymphatic vessel growth *in vivo* through regulation of Prox1 and VEGFR-3 expression; and 3) novel evidence demonstrating the suppression of Prox1 expression in p50 KO hepatocytes and neurons, suggesting for the first time that NF-κB p50 regulates Prox1 expression in cells other than LEC. Finally, these data advanced our basic understanding of molecular mechanisms governing postnatal lymphatic development and highlight the diverse roles of the NF-κB p50 subunit in normal physiology of both endothelial and non-endothelial tissues.

Reference List

1. Ben Baruch A. Host microenvironment in breast cancer development: inflammatory cells, cytokines and chemokines in breast cancer progression: reciprocal tumor-microenvironment interactions. *Breast Cancer Res.* 2003;5(1):31-36.

2. Yu JL, Rak JW. Host microenvironment in breast cancer development: inflammatory and immune cells in tumour angiogenesis and arteriogenesis. *Breast Cancer Res.* 2003;5(2):83-88.

3. Schoppmann SF, Horvat R, Birner P. Lymphatic vessels and lymphangiogenesis in female cancer: mechanisms, clinical impact and possible implications for anti-lymphangiogenic therapies (Review). *Oncol Rep.* 2002;9(3):455-460.

4. Mouta C, Heroult M. Inflammatory triggers of lymphangiogenesis. *Lymphat Res Biol.* 2003;1(3):201-218.

5. Chakrabarti R, Subramaniam V, Abdalla S, Jothy S, Prud'homme GJ. Tranilast inhibits the growth and metastasis of mammary carcinoma. *Anticancer Drugs.* 2009;20(5):334-345.

6. Veikkola T, Jussila L, Makinen T et al. Signalling via vascular endothelial growth factor receptor-3 is sufficient for lymphangiogenesis in transgenic mice. *EMBO J.* 2001;20(6):1223-1231.

7. Kaipainen A, Korhonen J, Mustonen T et al. Expression of the fms-like tyrosine kinase 4 gene becomes restricted to lymphatic endothelium during development. *Proc Natl Acad Sci U S A.* 1995;92(8):3566-3570.

8. Whitehurst B, Flister MJ, Bagaitkar J et al. Anti-VEGF-A therapy reduces lymphatic vessel density and expression of VEGFR-3 in an orthotopic breast tumor model. *Int J Cancer.* 2007;121(10):2181-2191.

9. Paavonen K, Puolakkainen P, Jussila L, Jahkola T, Alitalo K. Vascular endothelial growth factor receptor-3 in lymphangiogenesis in wound healing. *Am J Pathol.* 2000;156(5):1499-1504.

10. Baluk P, Tammela T, Ator E et al. Pathogenesis of persistent lymphatic vessel hyperplasia in chronic airway inflammation. *J Clin Invest.* 2005;115(2):247-257.

11. Kunstfeld R, Hirakawa S, Hong YK et al. Induction of cutaneous delayed-type hypersensitivity reactions in VEGF-A transgenic mice results in chronic skin inflammation associated with persistent lymphatic hyperplasia. *Blood.* 2004;104(4):1048-1057.

12. Zhang Q, Lu Y, Proulx ST et al. Increased lymphangiogenesis in joints of mice with inflammatory arthritis. *Arthritis Res Ther.* 2007;9(6):R118.

13. Maruyama K, Ii M, Cursiefen C et al. Inflammation-induced lymphangiogenesis in the cornea arises from CD11b-positive macrophages. *J Clin Invest.* 2005;115(9):2363-2372.

14. Cursiefen C, Chen L, Borges LP et al. VEGF-A stimulates lymphangiogenesis and hemangiogenesis in inflammatory neovascularization via macrophage recruitment. *J Clin Invest.* 2004;113(7):1040-1050.

15. Iwata C, Kano MR, Komuro A et al. Inhibition of cyclooxygenase-2 suppresses lymph node metastasis via reduction of lymphangiogenesis. *Cancer Res.* 2007;67(21):10181-10189.

16. Ristimaki A, Narko K, Enholm B, Joukov V, Alitalo K. Proinflammatory cytokines regulate expression of the lymphatic endothelial mitogen vascular endothelial growth factor-C. *J Biol Chem.* 1998;273(14):8413-8418.

17. Goldman J, Rutkowski JM, Shields JD et al. Cooperative and redundant roles of VEGFR-2 and VEGFR-3 signaling in adult lymphangiogenesis. *FASEB J.* 2007;21(4):1003-1012.

18. Roberts N, Kloos B, Cassella M et al. Inhibition of VEGFR-3 activation with the antagonistic antibody more potently suppresses lymph node and distant metastases than inactivation of VEGFR-2. *Cancer Res.* 2006;66(5):2650-2657.

19. Hong YK, Harvey N, Noh YH et al. Prox1 is a master control gene in the program specifying lymphatic endothelial cell fate. *Dev Dyn.* 2002;225(3):351-357.

20. Wigle JT, Harvey N, Detmar M et al. An essential role for Prox1 in the induction of the lymphatic endothelial cell phenotype. *EMBO J.* 2002;21(7):1505-1513.

21. Petrova TV, Makinen T, Makela TP et al. Lymphatic endothelial reprogramming of vascular endothelial cells by the Prox-1 homeobox transcription factor. *EMBO J.* 2002;21(17):4593-4599.

22. Mishima K, Watabe T, Saito A et al. Prox1 induces lymphatic endothelial differentiation via integrin alpha9 and other signaling cascades. *Mol Biol Cell.* 2007;18(4):1421-1429.

23. Groger M, Loewe R, Holnthoner W et al. IL-3 induces expression of lymphatic markers Prox-1 and podoplanin in human endothelial cells. *J Immunol.* 2004;173(12):7161-7169.

24. Karin M. Nuclear factor-kappaB in cancer development and progression. *Nature.* 2006;441(7092):431-436.

25. Beinke S, Ley SC. Functions of NF-kappaB1 and NF-kappaB2 in immune cell biology. *Biochem J.* 2004;382(Pt 2):393-409.

26. Kiriakidis S, Andreakos E, Monaco C et al. VEGF expression in human macrophages is NF-kappaB-dependent: studies using adenoviruses expressing the endogenous NF-kappaB inhibitor IkappaBalpha and a kinase-defective form of the IkappaB kinase 2. *J Cell Sci.* 2003;116(Pt 4):665-674.

27. Tsai PW, Shiah SG, Lin MT, Wu CW, Kuo ML. Up-regulation of vascular endothelial growth factor C in breast cancer cells by heregulin-beta 1. A critical role of p38/nuclear factor-kappa B signaling pathway. *J Biol Chem.* 2003;278(8):5750-5759.

28. Kataru RP, Jung K, Jang C et al. Critical role of CD11b+ macrophages and VEGF in inflammatory lymphangiogenesis, antigen clearance, and inflammation resolution. *Blood.* 2009;113(22):5650-5659.

29. Baluk P, Tammela T, Ator E et al. Pathogenesis of persistent lymphatic vessel hyperplasia in chronic airway inflammation. *J Clin Invest.* 2005;115(2):247-257.

30. Kunstfeld R, Hirakawa S, Hong YK et al. Induction of cutaneous delayed-type hypersensitivity reactions in VEGF-A transgenic mice results in chronic skin inflammation associated with persistent lymphatic hyperplasia. *Blood.* 2004;104(4):1048-1057.

31. Guo R, Zhou Q, Proulx ST et al. Inhibition of lymphangiogenesis and lymphatic drainage via vascular endothelial growth factor receptor 3 blockade increases the severity of inflammation in a mouse model of chronic inflammatory arthritis. *Arthritis Rheum.* 2009;60(9):2666-2676.

32. Klement G, Huang P, Mayer B et al. Differences in therapeutic indexes of combination metronomic chemotherapy and an anti-VEGFR-2 antibody in multidrug-resistant human breast cancer xenografts. *Clin Cancer Res.* 2002;8(1):221-232.

33. Sledge GW, Jr., Miller KD. Metastatic breast cancer: the role of chemotherapy. *Semin Oncol.* 1999;26(1 Suppl 2):6-10.

34. Gotaskie GE, Andreassi BF. Paclitaxel: a new antimitotic chemotherapeutic agent. *Cancer Pract.* 1994;2(1):27-33.

35. Witmer AN, Dai J, Weich HA, Vrensen GF, Schlingemann RO. Expression of vascular endothelial growth factor receptors 1, 2, and 3 in quiescent endothelia. *J Histochem Cytochem.* 2002;50(6):767-777.

36. Veikkola T, Jussila L, Makinen T et al. Signalling via vascular endothelial growth factor receptor-3 is sufficient for lymphangiogenesis in transgenic mice. *EMBO J.* 2001;20(6):1223-1231.

37. Wigle JT, Oliver G. Prox1 function is required for the development of the murine lymphatic system. *Cell.* 1999;98(6):769-778.

38. Flister MJ, Wilber A, Hall KL et al. Inflammation induces lymphangiogenesis through up-regulation of VEGFR-3 mediated by NF-kappaB and Prox1. *Blood.* 2010;115(2):418-429.

39. Mouta CC, Nasser SM, di TE et al. LYVE-1 is not restricted to the lymph vessels: expression in normal liver blood sinusoids and down-regulation in human liver cancer and cirrhosis. *Cancer Res.* 2001;61(22):8079-8084.

40. Hou Y, Li F, Karin M, Ostrowski MC. Analysis of the IKKbeta/NF-kappaB signaling pathway during embryonic angiogenesis. *Dev Dyn.* 2008;237(10):2926-2935.

41. Oliver G, Sosa-Pineda B, Geisendorf S et al. Prox 1, a prospero-related homeobox gene expressed during mouse development. *Mech Dev.* 1993;44(1):3-16.

42. Risebro CA, Searles RG, Melville AA et al. Prox1 maintains muscle structure and growth in the developing heart. *Development.* 2009;136(3):495-505.

43. Lavado A, Oliver G. Prox1 expression patterns in the developing and adult murine brain. *Dev Dyn.* 2007;236(2):518-524.

44. Valtola R, Salven P, Heikkila P et al. VEGFR-3 and its ligand VEGF-C are associated with angiogenesis in breast cancer. *Am J Pathol.* 1999;154(5):1381-1390.

45. Tammela T, Zarkada G, Wallgard E et al. Blocking VEGFR-3 suppresses angiogenic sprouting and vascular network formation. *Nature.* 2008;454(7204):656-660.

46. Shawber CJ, Funahashi Y, Francisco E et al. Notch alters VEGF responsiveness in human and murine endothelial cells by direct regulation of VEGFR-3 expression. *J Clin Invest.* 2007;117(11):3369-3382.

47. Hallmann R, Mayer DN, Berg EL, Broermann R, Butcher EC. Novel mouse endothelial cell surface marker is suppressed during differentiation of the blood brain barrier. *Dev Dyn.* 1995;202(4):325-332.

48. Zhang J, Warren MA, Shoemaker SF, Ip MM. NFkappaB1/p50 is not required for tumor necrosis factor-stimulated growth of primary mammary epithelial cells: implications for NFkappaB2/p52 and RelB. *Endocrinology.* 2007;148(1):268-278.

49. Banerji S, Ni J, Wang SX et al. LYVE-1, a new homologue of the CD44 glycoprotein, is a lymph-specific receptor for hyaluronan. *J Cell Biol.* 1999;144(4):789-801.

50. Mancuso MR, Davis R, Norberg SM et al. Rapid vascular regrowth in tumors after reversal of VEGF inhibition. *J Clin Invest.* 2006;116(10):2610-2621.

51. Schmittgen TD, Livak KJ. Analyzing real-time PCR data by the comparative C(T) method. *Nat Protoc.* 2008;3(6):1101-1108.

Apendinx A

Inflammation induces lymphangiogenesis through up-regulation of VEGFR-3 mediated by NF-κB and Prox1

Michael J. Flister,[1] Andrew Wilber,[1,2] Kelly L. Hall,[1] Caname Iwata,[3] Kohei Miyazono,[3] Riccardo E. Nisato,[4] Michael S. Pepper,[5] David C. Zawieja,[6] and Sophia Ran[1]

Departments of [1]Medical Microbiology, Immunology, and Cell Biology and [2]Surgery, Southern Illinois University School of Medicine, Springfield; [3]Department of Molecular Pathology, Graduate School of Medicine, University of Tokyo, Tokyo, Japan; [4]Department of Cell Physiology and Metabolism, University Medical Center, Geneva, Switzerland; [5]Netcare Institute of Cellular and Molecular Medicine, Pretoria, South Africa; and [6]Department of Systems Biology and Translational Medicine, Cardiovascular Research Institute, Texas A&M Health Science Center, College Station

The concept of inflammation-induced lymphangiogenesis (ie, formation of new lymphatic vessels) has long been recognized, but the molecular mechanisms remained largely unknown. The 2 primary mediators of lymphangiogenesis are vascular endothelial growth factor receptor-3 (VEGFR-3) and Prox1. The key factors that regulate inflammation-induced transcription are members of the nuclear factor-kappaB (NF-κB) family; however, the role of NF-κB in regulation of lymphatic-specific genes has not been defined. Here, we identified VEGFR-3 and Prox1 as downstream targets of the NF-κB pathway. In vivo time-course analysis of inflammation-induced lymphangiogenesis showed activation of NF-κB followed by sequential up-regulation of Prox1 and VEGFR-3 that preceded lymphangiogenesis by 4 and 2 days, respectively. Activation of NF-κB by inflammatory stimuli also elevated Prox1 and VEGFR-3 expression in cultured lymphatic endothelial cells, resulting in increased proliferation and migration. We also show that Prox1 synergizes with the p50 of NF-κB to control VEGFR-3 expression. Collectively, our findings suggest that induction of the NF-κB pathway by inflammatory stimuli activates Prox1, and both NF-κB and Prox1 activate the VEGFR-3 promoter leading to increased receptor expression in lymphatic endothelial cells. This, in turn, enhances the responsiveness of preexisting lymphatic endothelium to VEGFR-3 binding factors, VEGF-C and VEGF-D, ultimately resulting in robust lymphangiogenesis. (Blood. 2010;115: 418-429)

Introduction

The lymphatic vascular system has multiple functions in normal physiology including regulation of interstitial pressure,[1] lipid absorption,[2] immune surveillance,[1] and resolution of inflammation.[3] The formation of new lymphatic vessels (ie, lymphangiogenesis) is dynamic during embryogenesis but is relatively rare and selectively regulated in adulthood. Insufficient development of postnatal lymphatic vessels impairs immune function and causes tissue edema,[1] whereas excessive lymphangiogenesis is associated with malignancy and strongly implicated in lymphatic metastasis.[4]

The key protein that regulates lymphangiogenesis is vascular endothelial growth factor receptor-3 (VEGFR-3),[5] a tyrosine kinase receptor expressed primarily in lymphatic endothelial cells (LECs).[6] VEGFR-3 signaling is activated upon binding of vascular endothelial growth factor-C (VEGF-C) or the related factor, VEGF-D.[5] In adulthood, lymphangiogenesis and elevated VEGFR-3 expression coincide with inflammatory conditions including cancer,[7] wound healing,[8] and chronic inflammatory diseases. Increased lymphatic vessel density (LVD) has been documented in chronic airway infection,[9] psoriasis,[10] arthritis,[11] and corneal injury.[12] VEGF-C and VEGF-D are elevated during inflammation, being produced by a variety of cells residing at inflamed sites, including macrophages,[9,13,14] dendritic cells, neutrophils,[9] mast cells, fibroblasts,[15] and tumor cells.[14] Inflammation-induced lymphatic hyperplasia and lymphangiogenesis are likely the result of increased VEGFR-3 expression that amplifies response to VEGF-C/-D. This is supported by observations that blocking VEGFR-3 signaling inhibits lymphangiogenesis during chronic inflammation,[9] wound healing,[16] and malignancy.[17]

Lymphangiogenesis is also regulated by the lymphatic-specific transcription factor, Prospero-related homeobox-1 (Prox1)[18,19] that specifies LEC fate by regulating expression of VEGFR-3[19] and other lymphatic-specific proteins during embryogenesis. The central role of Prox1 in developmental lymphangiogenesis suggests a similar role for Prox1 in adulthood. Studies have shown that Prox1 induces VEGFR-3 in adult blood vascular endothelial cells (BECs),[18,20] whereas silencing Prox1 in adult LECs down-regulates VEGFR-3 expression.[20,21] Prox1 has been shown to be up-regulated by inflammatory cytokines[22] and to colocalize with VEGFR-3 in lymphatic vessels. However, the role of Prox1 in regulation of VEGFR-3 expression during inflammation in vivo is unknown.

The primary mediators of the inflammatory response are dimeric transcription factors that belong to the nuclear factor-kappaB (NF-κB) family consisting of RelA (p65), NF-κB1 (p50), RelB, c-Rel, and NF-κB2 (p52).[23] The main NF-κB protein complexes that regulate the transcription of responsive genes are p50/p65 heterodimers or p50 and p65 homodimers.[24] More than

Submitted December 29, 2008; accepted October 13, 2009. Prepublished online as *Blood* First Edition paper, November 9, 2009; DOI 10.1182/blood-2008-12-196840.

The online version of this article contains a data supplement.

The publication costs of this article were defrayed in part by page charge payment. Therefore, and solely to indicate this fact, this article is hereby marked "advertisement" in accordance with 18 USC section 1734.

450 NF-κB–inducible genes have been identified, including proteins that mediate inflammation, immunity, tumorigenesis, and angiogenesis.[23] Several NF-κB–regulated genes stimulate lymphangiogenesis either directly (eg, VEGF-A[25] and VEGF-C[26]) or indirectly, by up-regulating VEGF-C and VEGF-D (eg, IL-1β,[15] TNF-α,[15] and COX-2[14]). Activated NF-κB signaling coincides with increased VEGFR-3$^+$ lymphatics during inflammation,[9] suggesting a role for NF-κB in regulation of VEGFR-3 expression.

Although extensive evidence supports the link between inflammation and lymphangiogenesis, the molecular mechanisms underlying this association are largely unknown. We postulate that NF-κB, the main intracellular mediator of inflammation, regulates transcription of key mediators of lymphangiogenesis, VEGFR-3 and Prox1. To test this hypothesis, we used a mouse model of inflammatory peritonitis,[14] which showed that lymphangiogenesis is preceded by increased VEGFR-3 and Prox1 expression on preexisting inflamed lymphatic vessels. Analysis of the human VEGFR-3 promoter showed transcriptional regulation by p50, p65, and Prox1. These data demonstrate for the first time that NF-κB and Prox1 induce VEGFR-3 transcription, indicating the important roles for both factors in the regulation of VEGFR-3–dependent inflammatory lymphangiogenesis in vivo.

Methods

Materials

Human Prox1 CDS ligated into pCMV6-XL6 (pCMV-Prox1) plasmid was purchased from OriGene. NF-κB plasmids, pCMV-Flag-p50 and pCMV-Flag-p65, were kindly provided by Dr Albert Baldwin (University of North Carolina, Chapel Hill). Promoter-luciferase reporter plasmids for ubiquitin C and phosphoglycerate kinase were described previously.[27] Lipopolysaccharide (LPS) was purchased from Sigma-Aldrich. Rat VEGFR-3–specific ligand, VEGF-C152S, and human interleukin-3 (IL-3) were purchased from Peprotech. Pyrrolidine dithiocarbamate (PDTC) and MG-132 were purchased from Calbiochem. Leptomycin B was from LC Laboratories.

Antibodies

Primary antibodies used in this study were: goat anti–mVEGFR-3 and anti-Prox1 (R&D Systems); rabbit anti-p65, anti-pp65, anti-p50, and anti-pp50 (Santa Cruz); rabbit anti–mLYVE-1 and anti-Prox1 (AngioBio); rabbit anti–Ki-67 (Biomeda); goat anti–acetylated-histone-H3 (Upstate); mouse anti-Flag (ABM); mouse anti–β-actin (JLA20; Developmental Studies Hybridoma Bank); and rabbit anti–VEGF-C (Invitrogen). Secondary horseradish peroxidase–, fluorescein isothiocyanate–, and Cy3-conjugated donkey anti–rabbit and anti–goat antibodies and nonspecific rabbit immunoglobulin G (IgG) were from Jackson ImmunoResearch Laboratories.

Cell lines

Rat LECs (RLECs) were isolated and cultured as previously described.[28] Human embryonic kidney cells (HEK293) were cultured in Dulbecco modified Eagle medium (DMEM) with 10% fetal bovine serum (FBS). Human primary LECs (H-LLY) and immortalized human dermal LECs ($HDLEC_{htert}$)[29] were cultured in gelatin-coated flasks in microvascular endothelial cell growth medium-2 (EGM-2MV) medium (Clonetics). Human lung microvascular endothelial cells (HULECs) were obtained from the Centers for Disease Control and Prevention.

Mouse peritonitis model

All mice experiments were approved by Southern Illinois University School of Medicine Institutional Laboratory Animal Care and Use Committee. Female BALB/c mice (3-6 months) were obtained from The Jackson Laboratory and treated in accordance with institutional guidelines. Peritonitis was induced by 0.5-mL intraperitoneal injections of 1.5% sodium thioglycollate (vol/vol in saline; BD Biosciences) for 2 weeks, as previously described.[14] For time-course analysis, mice (3-4 per group) received thioglycollate (TG) every 48 hours for the indicated periods. Control mice were injected intraperitoneally with 0.5 mL of saline. Diaphragms were removed after a 2-week treatment, fixed with 10 N of Mildform for 1 hour at room temperature, bathed in 30% sucrose overnight, and snap-frozen.

Immunohistochemistry

Frozen 8-μm sections were fixed with acetone for 10 minutes, washed in phosphate-buffered saline plus Tween-20 (pH 7.4, 0.1% Tween-20) for 10 minutes and incubated for 1 hour at 37°C with primary antibodies (diluted 1:100) against VEGFR-3, LYVE-1, Prox1, or Ki-67, followed by appropriate fluorescein isothiocyanate– or Cy3-conjugated secondary antibodies (diluted 1:100) for 1 hour at 37°C. For double immunofluorescent staining, sections were incubated with each primary and secondary antibody for 1 hour at 37°C and washed for 10 minutes in phosphate-buffered saline plus Tween-20 between steps. Slides were mounted in Vectashield medium containing 4,6′-diamidino-2-phenylindole (4,6 diamidino-2-phenylindole) nuclear stain (Vector Labs). Images were acquired on an Olympus BX41 upright microscope equipped with a DP70 digital camera and DP Controller software (Olympus).

Immunofluorescent intensity measurements

Analysis of VEGFR-3 and LYVE-1 double-staining was performed as described by Tammela et al,[30] with slight modifications. In brief, diaphragm sections were double-stained with goat anti–mVEGFR-3 and rabbit anti–mLYVE-1 antibodies. Fluorescent images were acquired at a constant exposure time at 400× magnification on an Olympus IX71 inverted microscope (Olympus) equipped with a Retiga Exi charge-coupled device camera (QImaging). Diaphragms stained with secondary antibodies alone were used to set the exposure time. Images acquired at a constant exposure time were converted to 12-bit gray scale followed by outlining vascular structures and analysis with Image-Pro Software (Media Cybernetics). Supplemental Figure 1 (available on the *Blood* website; see the Supplemental Materials link at the top of the online article) shows an example of image acquisition and vessel outlining. All images were within a linear intensity range between 0 and 4095. To exclude nonspecific staining, structures less than 10 μm (1 μm = 6.4 pixels) in diameter were excluded. To calculate mean vessel intensity, the sums of pixel intensities per vessel were divided by total vessel area (μm^2). Mean vessel intensities from 5 to 10 images per diaphragm (n = 3 per group) were averaged and compared between treated and control groups.

Western blot analysis

Cells were lysed in ice-cold buffer [50mM tris (hydroxymethyl)aminomethane-HCl, pH 7.5, 150mM NaCl, 1mM ethylenediaminetetraacetic acid, 1% Triton-X100, 0.1% sodium dodecyl sulfate, phenylmethylsulphonyl fluoride 1:100, and protease inhibitor cocktail 1:50]. Proteins separated in 12% sodium dodecyl sulfate–polyacrylamide gel were transferred onto nitrocellulose membranes followed by overnight incubation with primary antibodies against p50, p65, Prox1, LYVE-1, VEGFR-3, Flag-tag, or β-actin; 1-hour incubation with horseradish peroxidase–conjugated secondary antibodies; and development with enhanced chemiluminescence reagent (Pierce). Protein bands were visualized using a Fujifilm LAS-3000 camera and analyzed with Image-Reader LAS-3000 software.

VEGFR-3 promoter cloning

Segments of −849 bp, −514 bp, −341 bp, −331 bp, −118 bp, and −46 bp of the 5′ untranslated region of VEGFR-3 and +55 bp of exon 1 were amplified by polymerase chain reaction (PCR) from a human genomic bacterial artificial chromosome (BAC) clone, CTD-2546M13 (Open Biosystems). Promoter segments spanning −436/−254 bp and −849/−254 bp (Δ309) were also PCR-amplified. Products were cloned into the pGL4 basic vector (Promega) to produce VEGFR-3 promoter-luciferase constructs. All

clones were sequenced and verified through comparison with published genomic sequence. Human VEGFR-3 promoter sequence (GenBank accession no. DQ911346[31]) was analyzed using MatInspector (http://www.genomatix.de/products/MatInspector/index.html[32]) and compared with published transcription factor binding sites.

Assay for VEGFR-3 promoter activity

Cells were transfected with 1 μg of DNA composed of 0.96 μg of promoter construct and 0.04 μg of Herpes simplex thymidine-kinase promoter–driven renilla luciferase (Promega) mixed with 3 μL of ExGen500 (Fermentas). After 24 hours, cells were lysed with 0.2% Triton-X100, and firefly and renilla luciferase activities were measured by a dual-luciferase assay performed according to manufacturer's protocol. Promoter-firefly luciferase activity was normalized per renilla activity or milligram of total protein.

Inflammatory stimulation of LECs

$HDLECs_{htert}$ were seeded in 6-well plates (200 000 cells/well) in 0.5% EGM2 medium (Lonza). Medium was replaced daily during a 72-hour time period, before treatment with IL-3 (10 ng/mL) or LPS (100 ng/mL) for 6 or 24 hours. RNA extraction and analysis of transcripts by quantitative reverse-transcription (qRT)–PCR was performed as described in "RT-PCR and qRT-PCR."

Cell proliferation and migration assays

RLECs were seeded in DMEM containing 1.5% FBS in 24-well plates at the density of 50 000 cells/well. IL-3 (5-100 ng/mL), LPS (50-1000 ng/mL), and VEGF-C152S (25-200 ng/mL) were added 2 hours after seeding. The effect of combined cytokines was measured after stimulation with VEGF-C152S (100 ng/mL) mixed with IL-3 (10 ng/mL) or LPS (500 ng/mL). After 72-hour incubation, cells were trypsinized and enumerated. The results are presented as the averaged cell number per well derived from 3 experiments performed in triplicate plus or minus SEM.

Cell migration was measured using 8 μm-pore Transwells according to the manufacturer's protocol (Corning). In brief, 50 000 RLECs were seeded in 0.25% DMEM on pre-equilibrated inserts. IL-3 (10 ng/mL), LPS (500 ng/mL), VEGF-C152S (200 ng/mL), or 0.25% FBS (negative control) was added to bottom chambers. After 24-hour incubation, inserts were washed, fixed in 2% paraformaldehyde for 10 minutes, and stained by crystal violet. Numbers of cells migrated per field were determined on 6 random images acquired at 200× and averaged.

ChIP

RLECs (2×10^7) were grown to 90% confluence and fixed with 1% formaldehyde. Cell lysis, shearing, and chromatin immunoprecipitation (ChIP) were performed using a ChIP-IT Express Kit according to the manufacturer's protocol (Active Motif). Chromatin was precipitated with anti-p50, p65, Prox1, acetylated-histone-H3 antibodies, or nonspecific rabbit IgG (negative control). Precipitated chromatin was amplified by PCR using primers for rat VEGFR-3 promoter listed in supplemental Table 1.

Suppression of p50/p65 expression by siRNA

Previously validated 21-nucleotide-long siRNA duplexes against p50 (sense strand, 5′-GGGGCUAUAAUCCUGGACUdTdT-3′)[33] and p65 (sense strand, 5′-GCCCUAUCCCUUUACGUCAdTdT-3′)[34] (Dharmacon) and predesigned Silencer Negative Control no. 1 siRNA (Ambion) were used for suppression of p50 and p65 expression. H-LLY cells were transfected with siRNA for 16 hours using siPORT NeoFX (Ambion) according to the manufacturer's protocol. Total RNA was isolated 48 hours after transfection and transcript levels were determined by qRT-PCR.

RT-PCR and qRT-PCR

Total RNA extracted by Tri-reagent was reverse transcribed using RTG You-Prime Reaction beads (Amersham) and random hexamer primers (Invitrogen). All primers used in this study are listed in supplemental Table 1. End point RT-PCR analysis was performed as previously described,[7] then visualized and analyzed using a FluroChem5500 imager (AlphaInnotech). qRT-PCR was performed using SYBR Master Mix and a 7500 Real-Time PCR machine from Applied Biosystems. Data were normalized to β-actin and relative mRNA expression was determined using the ΔΔCt method.

Statistical analysis

Statistical analysis was performed using SAS software (SAS Institute Inc). All results are expressed as mean plus or minus SEM. Differences in lymphatic vessel densities between groups were assessed by unpaired Student *t* test or Wilcoxon rank sum test. Intensity of VEGFR-3 and LYVE-1 staining per lymphatic vessels was assessed by analysis of variance for a nested design. Statistical significance was defined as *P* value less than .05.

Results

Inflammation induces lymphatic VEGFR-3 and Prox1 expression during lymphangiogenesis in vivo

Regulation of VEGFR-3 by inflammation is suggested by reports demonstrating inhibition of lymphangiogenesis by blockade of VEGFR-3 signaling.[9] Prox1 may also contribute to this process because it is induced by inflammatory mediators,[22] which coincides with elevated VEGFR-3.[35] However, the roles of VEGFR-3 and Prox1 in inflammatory lymphangiogenesis have not been demonstrated.

To analyze VEGFR-3 and Prox1 expression during inflammation, we induced peritonitis in Balb/c mice by TG injections, a method reported to induce lymphangiogenesis in the diaphragm.[14] Diaphragms from saline (control)– and TG-treated mice were removed after a 2-week treatment and stained for the lymphatic marker, LYVE-1, and VEGFR-3 (Figure 1). Consistent with previous studies,[14,36] the number of LYVE-1^+ lymphatic vessels increased by 1.9-fold (± 0.3-fold) in TG-treated mice compared with controls (Figure 1A-B). These tissues also showed a 4.5-fold (± 0.3-fold) increase in VEGFR-3^+ vessel density (Figure 1A,C). Coexpression of VEGFR-3 and LYVE-1 was quantified using the method described by Tammela et al[30] that measures the fluorescent intensity of target expression normalized per vascular area. This revealed a lymphatic-specific increase of VEGFR-3 (~ 67%) but not LYVE-1 (Figure 1D-E, supplemental Figure 3) expression, suggesting that inflammation increases both LVD and VEGFR-3 expression per individual vessel.

Prox1 reportedly regulates VEGFR-3 expression in cultured LECs[18,20]; however, a similar function in vivo has not been reported. We sought to determine Prox1 expression in VEGFR-3^+ lymphatic vessels during inflammation. Double-staining showed coincident up-regulation of VEGFR-3 and Prox1 in lymphatic vessels of inflamed diaphragms compared with control tissues (Figure 1F). Moreover, the frequency of Prox1^+ nuclei per lymphatic vessel area was increased by 3.3-fold (± 0.5-fold; Figure 1G).

To determine the proliferative status of VEGFR-3^+/Prox1^+ vessels, control and inflamed sections were costained for Ki-67 in combination with anti–VEGFR-3 or anti-Prox1 antibodies. Quiescent lymphatic vessels of control mice lacked Ki-67. In contrast, lymphatic vessels in TG-treated mice displayed widespread Ki-67 colocalized with both Prox1 and VEGFR-3 (Figure 1H). Collectively, these data demonstrate that inflammation induces VEGFR-3 and Prox1 expression on preexisting and sprouting lymphatic vessels.

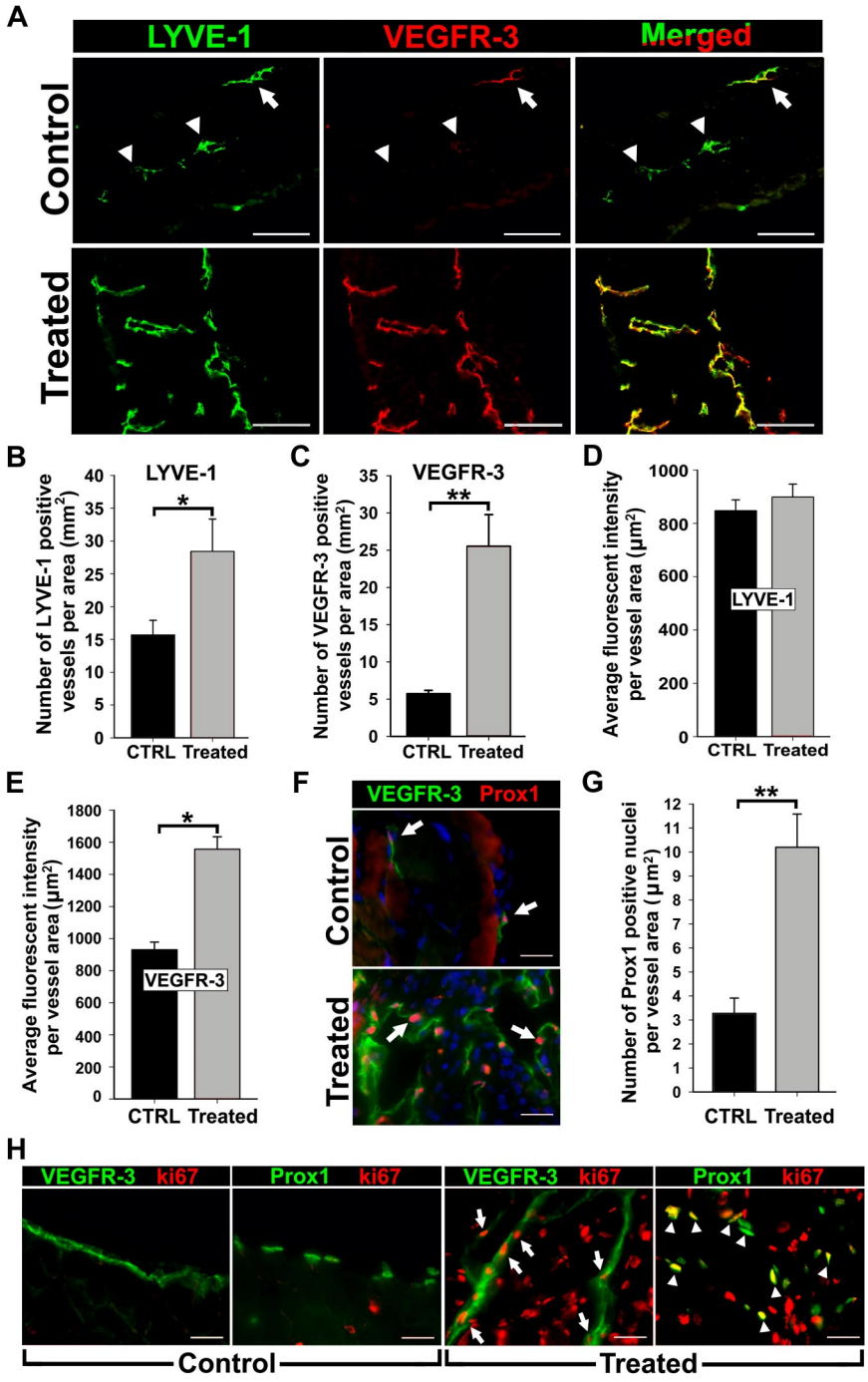

Figure 1. Inflammation induces VEGFR-3 and Prox1 expression in activated lymphatic vessels. Peritonitis was induced by repetitive intraperitoneal injections of thioglycollate (TG) every 48 hours for 2 weeks. (A) Diaphragms from mice treated for 2 weeks with TG to induce peritonitis or saline as a control (n = 3 mice per group) were double-stained with anti–LYVE-1 and anti–VEGFR-3 antibodies. Note strong expression and complete overlap of VEGFR-3 with LYVE-1 in inflamed tissues compared with quiescent lymphatic vessels in control sections with weakly detected (arrow) or absent (arrowheads) VEGFR-3. LYVE-1$^+$ (B) and VEGFR-3$^+$ (C) lymphatic vessels were counted on the entire diaphragm sections and the numbers were normalized per total section area expressed in square millimeters. The results are presented as the mean vessel density per group ± SEM. (B) *$P < .05$ versus control as determined by Wilcoxon rank sum test. (C) **$P < .01$ versus control as determined by Student unpaired *t* test. The mean fluorescent intensity (MFI) per vessel was analyzed on LYVE-1$^+$ (D) and VEGFR-3$^+$ (E) lymphatic vessels (5-10 vessels per diaphragm). MFI is expressed as relative units normalized per vascular area expressed in square micrometers. The mean MFI values ± SEM derived from 3 mice per group are shown. (E) *$P < .05$ versus control, as determined by nested analysis of variance described in "Statistical analysis." (F) Diaphragms from TG-treated and control mice were double-stained with anti-Prox1 and anti–VEGFR-3 antibodies. Arrows point to Prox1$^+$ nuclei. (G) Prox1$^+$ nuclei were enumerated and normalized per LYVE-1$^+$ lymphatic area (μm²) in diaphragms of TG- and saline-treated control mice. **$P < .01$ versus control as determined by Student unpaired *t* test. (H) Diaphragm sections were costained with antibodies against VEGFR-3 or Prox1 and a proliferative marker, Ki-67, to assess proliferative status of lymphatic vessels in the diaphragms of TG-treated or control mice. Note overlapping expression of Ki-67/VEGFR-3 (arrow) and Ki-67/Prox1 (arrowhead) detected in inflamed lymphatic vessels but absent from quiescent lymphatic vessels in control tissues. Scale bars represent 100 μm (A) and 20 μm (F,H).

Increased Prox1 and VEGFR-3 expression precedes lymphangiogenesis

LEC activation is associated with increased Prox1[37] and VEGFR-3,[5] yet their lymphatic-specific expression kinetics at early stages of lymphangiogenesis has not been examined. To determine the timeline of events leading to lymphangiogenesis, diaphragms from control and TG-treated mice harvested at days 1 to 4 and 7 after treatment were analyzed for expression of Prox1, VEGFR-3, and LYVE-1 by immunofluorescence and Western blot. Figure 2A and B show that compared with control tissues, the density of Prox1$^+$ lymphatic vessels increased (3.8-fold, $P < .001$) on the first day and remained significantly elevated (2.2- to 3.1-fold) on days 2 to 7. In contrast, the increase in VEGFR-3$^+$ vessel density became statistically significant only on day 4 (1.7-fold, $P < .05$) and day 7 (3.1-fold, $P < .01$, Figure 2C). During this period, LYVE-1$^+$ vessel density was unchanged except for an insignificant 1.6-fold increase on day 7 (Figure 2D). This immunofluorescent analysis showed that increased Prox1 expression precedes VEGFR-3 up-regulation by 2 to 3 days and elevation of both proteins precedes lymphangiogenesis.

Western blot analysis of actin-normalized protein expression of lymphatic markers as well as total and phosphorylated NF-κB p50 and p65 at different days after treatment confirmed this conclusion (Figure 2E). As expected, p50, p65, p-p50, and p-p65 were induced by inflammation with the most pronounced changes detected in p-p50 on the first day of treatment. NF-κB increase was mirrored

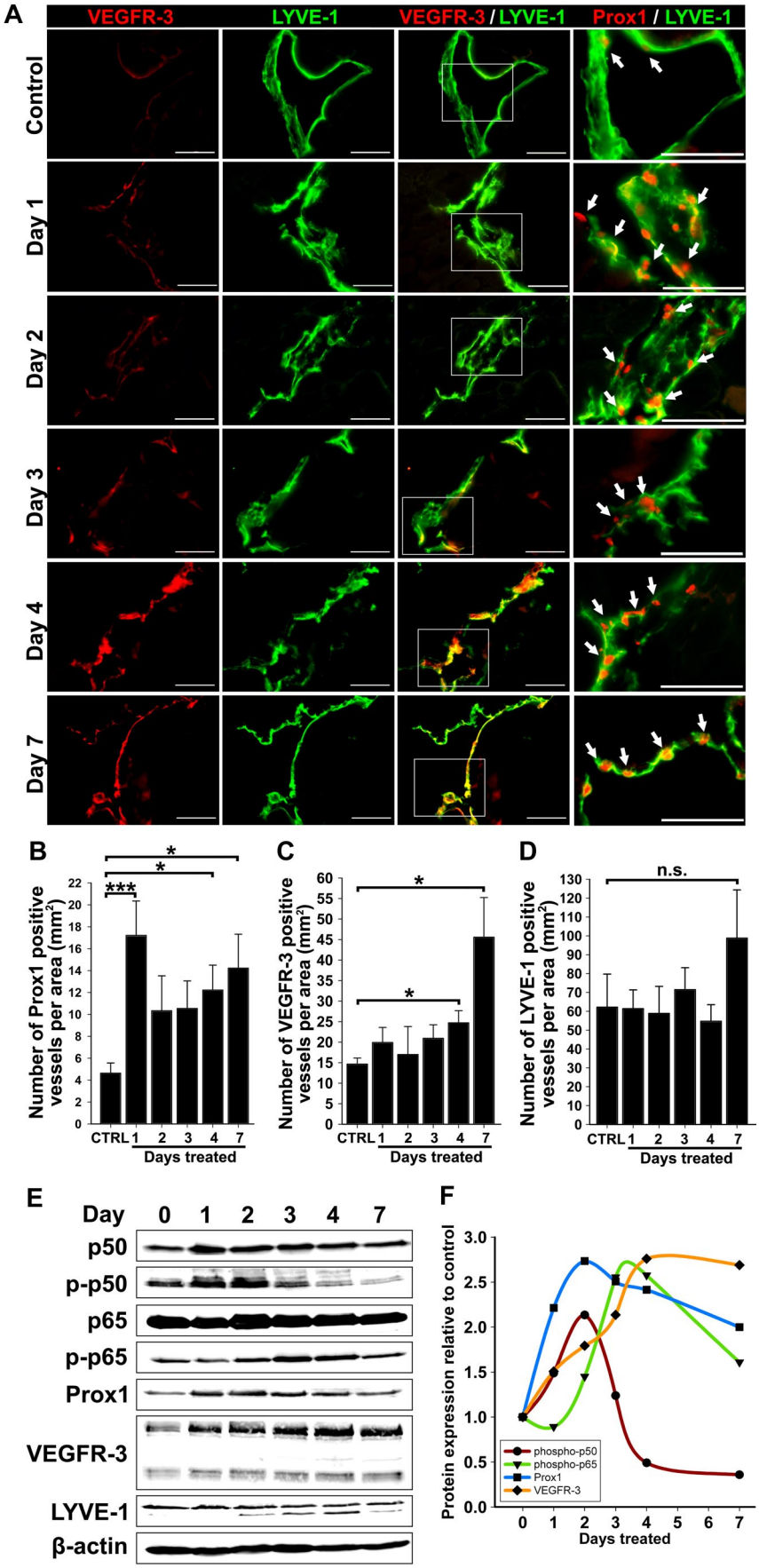

Figure 2. Up-regulation of VEGFR-3 and Prox1 precedes new lymphatic vessel formation during inflammation. (A) Double immunostaining of VEGFR-3/LYVE-1 and Prox1/LYVE-1 in serial diaphragm sections derived from mice treated with saline or TG (n = 3-4 mice per group) and harvested 1, 2, 3, 4, and 7 days after onset of treatment. Scale bars represent 50 μm. Lymphatic vessels shown are representative of whole diaphragm sections from 3 to 4 mice per group. (B-D) Quantification of Prox1-positive (B), VEGFR-3—positive (C), and LYVE-1—positive (D) vessels normalized per area of the entire diaphragm section measured in square millimeters. Quantitative analysis was performed on diaphragms harvested from 3 to 4 mice per group at indicated days after the first TG or saline injection. Data are presented as the mean number of vessels per diaphragm section ± SEM; ns denotes nonsignificant changes; *$P < .05$ and ***$P < .01$ versus control, as determined by Student unpaired t test. (E) Protein expression of Prox1, VEGFR-3, LYVE-1, NF-κB p50 phosphorylated on Ser337, nonphosphorylated NF-κB p50, NF-κB p65 phosphorylated on Ser276, nonphosphorylated NF-κB p65, and β-actin was determined by Western blot of combined lysates (100 μg of total protein per lane) derived from 3 to 4 mice per group. (F) Protein expression in Western blots was determined by band densitometry. Values were normalized to β-actin and are shown as fold increase relative to expression of corresponding proteins in untreated control mice at day 0.

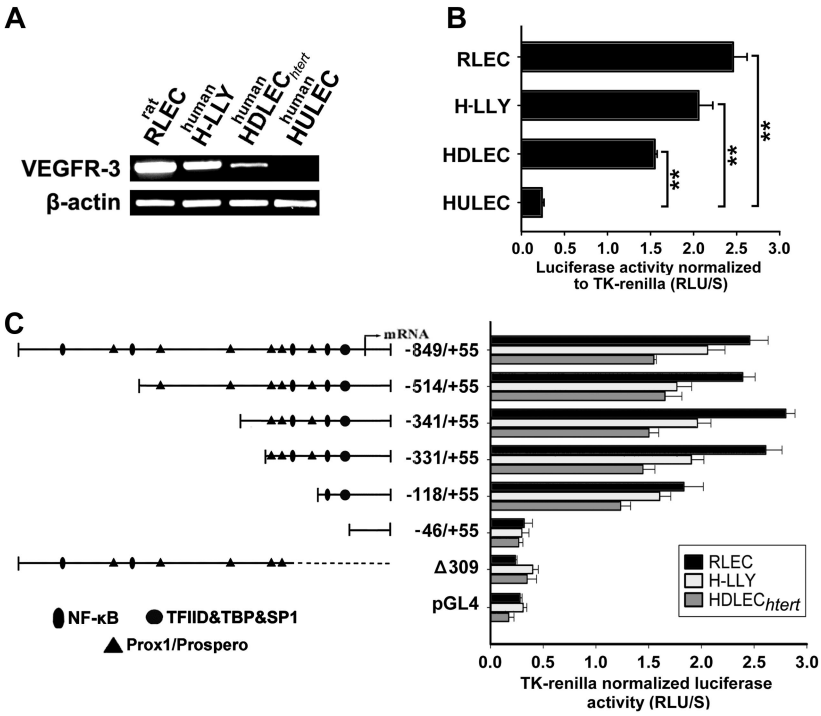

Figure 3. VEGFR-3 promoter characterization and gene expression in lymphatic endothelial cells. (A) VEGFR-3 mRNA expression and (B) full-length VEGFR-3$^{-849/+55}$ promoter activity were measured in the lymphatic endothelial cell lines RLECs, H-LLY, and HDLECs$_{htert}$. Human lung blood microvascular endothelial cell line, HULEC, was used as a VEGFR-3–negative cell line. Data shown are a representative image of VEGFR-3 transcript expression of 3 independent experiments (A) and the mean promoter activity of 3 independent experiments ± SEM (B). $^{**}P < .01$ versus VEGFR-3 promoter activity in the negative control cell line HULEC as determined by Student unpaired *t* test. (C) Activities of VEGFR-3 promoter deletion constructs were tested in RLECs, H-LLY, and HDLECs$_{htert}$. The left panel shows schematic illustration of deletion constructs with relative locations of predicted transcription factor binding sites. The right panel shows VEGFR-3 promoter activity of deletion constructs presented as relative light units per second (RLU/S) normalized per renilla luciferase activity of cotransfected thymidine kinase (TK)–renilla plasmid. Experiments were performed in duplicate and reproduced at least 3 times. Data are presented as the mean promoter activity of 3 independent experiments ± SEM.

by Prox1 up-regulation that doubled on day 1 of inflammation and nearly tripled on day 2 (Figure 2F). In contrast, the peak of VEGFR-3 expression was delayed to day 4, on which its level in inflamed tissues was 2.8-fold higher compared with controls (supplemental Table 2). Consistent with immunostaining, no changes in LYVE-1 protein were detected over 7 days of treatment. These data suggest that activation of NF-κB and Prox1 might be responsible for LEC activation, VEGFR-3 elevation, and lymphangiogenesis. Because no significant changes in LVD were detected in the first week of inflammation, these findings imply that NF-κB, Prox1, and VEGFR-3 are all required for lymphangiogenesis that is preceded by up-regulation of these proteins by 3 to 5 days.

Characterization of the human VEGFR-3 regulatory elements

To gain further insights into inflammation-dependent induction of VEGFR-3, we cloned and characterized the human VEGFR-3 promoter. Previous testing of the mouse VEGFR-3 promoter[38] demonstrated that the proximal 0.8 kb is sufficient to mediate cell type–specific transcriptional activity. However, NF-κB– and Prox1-dependent regulation of human or mouse promoter has not been previously examined.

High activity of the VEGFR-3$^{-849/+55}$ promoter was detected in 3 LEC lines with endogenous VEGFR-3 expression (Figure 3A). Promoter activity in LECs was 10.25-fold (± 0.7-fold; RLECs), 8.6-fold (± 0.7-fold; H-LLY), and 6.5-fold (± 0.2-fold; HDLECs$_{htert}$) higher than in the human blood vascular endothelial line, HULEC (Figure 3B). Promoter-reporter specificity was confirmed by empty vector and a promoter construct lacking the transcription start site (Δ309), both of which had 10% of the activity mediated by full-length VEGFR-3$^{-849/+55}$ (Figure 3C).

To identify the core elements required for transcriptional activity of the promoter we performed deletion analysis. Truncation from −849 bp to −331 bp did not significantly affect promoter activity (Figure 3C), suggesting that *cis*-acting response elements are located within the proximal −331/+55-bp region. Similar promoter activity was measured in human and rat LECs suggesting that the regulatory elements are conserved among species. Analysis of the −331/+55-bp region identified putative binding sites for several transcription factors including NF-κB and Prox1. Promoter truncation from −331 bp to −118 bp reduced activity by 15% to 30%, whereas reduction to −46 bp reduced luciferase activity to the level of control Δ309 construct (Figure 3C). This suggested that NF-κB and Prox1, whose binding sites are located within the proximal −331-bp region, are responsible for up-regulation of VEGFR-3 observed in vivo.

NF-κB transcription factors regulate VEGFR-3 expression in LECs

To determine the role of NF-κB in regulation of VEGFR-3 expression, LECs were cotransfected with the VEGFR-3$^{-849/+55}$ promoter and pCMV-Flag-p50, pCMV-Flag-p65, or empty plasmids. Equivalent expression of NF-κB subunits was determined by Western blot using Flag-specific antibody (supplemental Figure 4A). Compared with empty vector, NF-κB p65 activated VEGFR-3 promoter by 9-fold (± 1.0-fold) and 6-fold (± 0.5-fold) in H-LLY and RLECs, respectively. However, NF-κB p50 increased promoter activity by 58-fold (± 7-fold) and 51-fold (± 5-fold) in H-LLY and RLECs, respectively (Figure 4A). The difference in promoter activation was not due to functional deficiency of Flag-p65 construct as demonstrated by cotransfection with a NF-κB luciferase-reporter (supplemental Figure 4B). These data suggested that p50 has higher transactivation potential of VEGFR-3 promoter than p65 protein.

We used ChIP assay to determine whether NF-κB subunits bind the VEGFR-3 promoter. Primers were designed to encompass the region that includes or lacks the potential NF-κB sites. Only the −403/−238-bp promoter segment was detected by anti-p50, anti-p65, and anti–acetylated-H3 antibodies, indicating binding and active transcription by NF-κB in this region. ChIP analysis showed preferential binding by the p50 subunit (Figure 4B). Nonspecific rabbit IgG and primers flanking the region devoid of

NF-κB binding sites did not amplify PCR products, demonstrating specificity of the ChIP assay.

Inflammatory stimuli induce LEC proliferation and migration via VEGFR-3 signaling

Because the VEGFR-3 promoter was activated by NF-κB factors, we reasoned that treatment of LECs with NF-κB–dependent inflammatory mediators should increase the level of VEGFR-3 transcripts. To test this hypothesis, HDLECs$_{htert}$ were stimulated with known NF-κB activators, IL-3 (10 ng/mL) or LPS (100 ng/mL), for 6 and 24 hours, followed by qRT-PCR analysis of NF-κB p50 and p65, E-selectin, LYVE-1, and VEGFR-3 (Figure 4C-F). IL-3 and LPS treatment for 6 or 24 hours activated NF-κB signaling as demonstrated by significant increases in p50, p65, and E-selectin, a known NF-κB–regulated gene (Figure 4C-D). After 6 hours of treatment with LPS and IL-3, VEGFR-3 was up-regulated by 6.2-fold (± 0.8-fold) and 4.4-fold (± 0.7-fold), respectively. After 24 hours of treatment with these stimuli, VEGFR-3 was up-regulated by 1.6-fold (± 2.4-fold) and 2.9-fold (± 0.2-fold), respectively (Figure 4E). In comparison, LYVE-1 was unchanged by IL-3 or down-regulated after 24 hours of LPS treatment (Figure 4F), attesting to the target specificity of NF-κB stimulation.

We hypothesized that IL-3– and LPS-induced VEGFR-3 would enhance LEC proliferation and migration to VEGFR-3–specific ligands, such as, VEGF-C152S.[39] To test this hypothesis, we measured proliferation and migration of RLECs stimulated by IL-3 or LPS alone or in combination with VEGF-C152S. VEGF-C152S, IL-3, or LPS significantly increased RLEC proliferation in a dose-dependent manner, with maximum increase of 2.2-, 1.8-, and 2.4-fold compared with control, respectively (Figure 4G-I). Preactivation with IL-3 or LPS followed 6 hours later by VEGF-C152S treatment significantly increased proliferation by 18% to 39% compared with individual cytokines (Figure 4J). IL-3, LPS, or VEGF-C152S also induced RLEC migration by 2.1-, 1.6-, and 1.8-fold (Figure 4K). LEC migratory response to VEGF-C152S increased up to 44% after pretreatment with IL-3 or LPS (Figure 4K). These results suggest that VEGFR-3 up-regulation by inflammatory stimuli mediating NF-κB activation enhances LEC responsiveness to VEGFR-3–specific ligands.

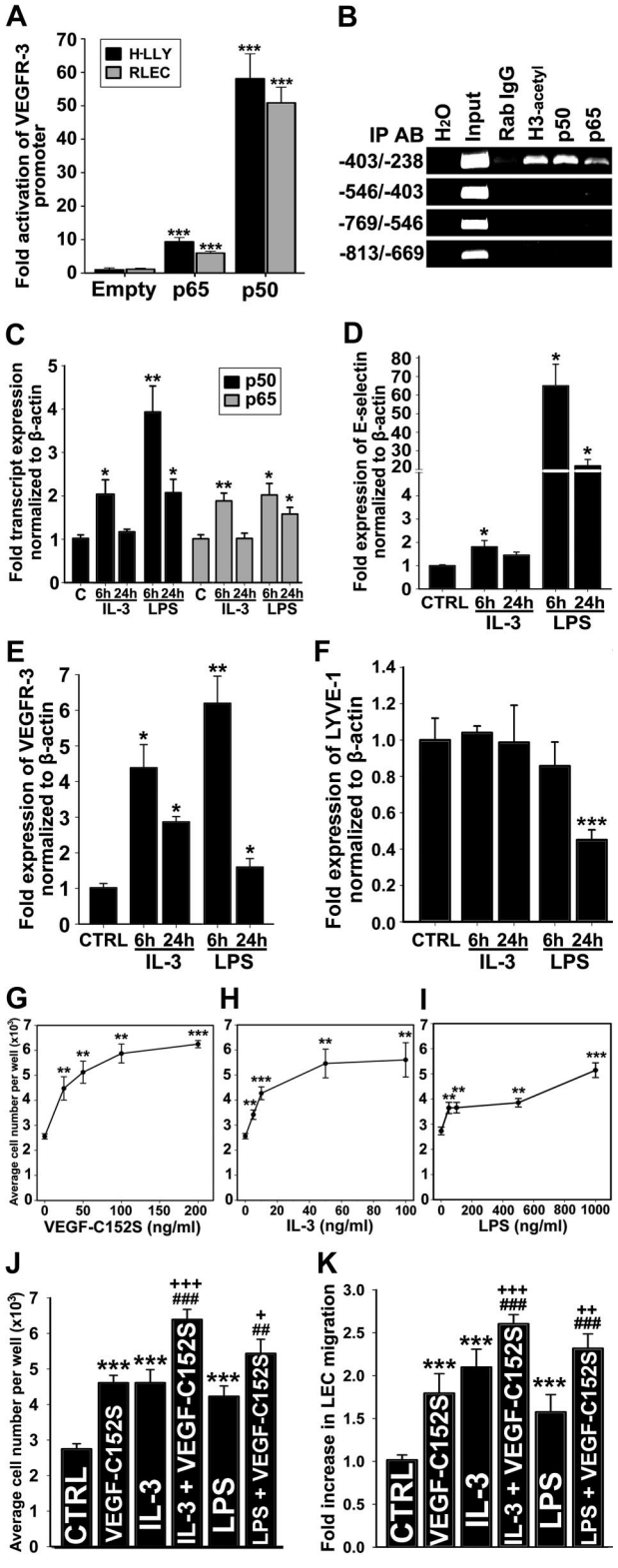

Figure 4. NF-κB pathway up-regulates VEGFR-3 expression and activates lymphatic endothelial cells. (A) VEGFR-3 promoter activity in RLECs and H-LLY cells cotransfected with VEGFR-3$^{-849/+55}$ and pCMV-Flag-p50, pCMV-Flag-p65, or empty control plasmids. Promoter activity is normalized per milligram of protein. Data presented for each cell line as the mean promoter activity ± SEM of 3 independent experiments performed in duplicate ± SEM (total n = 6 per experimental condition). ***$P < .001$ versus control as determined by Student unpaired *t* test. (B) ChIP was performed using RLECs and anti-p65, -p50, and -acetylated histone H3 antibodies (positive control), or nonspecific rabbit IgG (negative control). Immunoprecipitated chromatin was visualized by PCR using primers either flanking (−403/−238 bp) or upstream of putative NF-κB binding sites (−813/−403 bp). Data are representative of 4 independent ChIP experiments with similar results. (C-F) qRT-PCR analysis of NF-κB p50 and p65 (C), E-selectin (D), VEGFR-3 (E), and LYVE-1 (F) mRNA expression in HDLECs$_{htert}$ treated with IL-3 (10 ng/mL) or LPS (100 ng/mL) for 6 or 24 hours. The relative expression of each target was normalized to β-actin. Data are presented as the mean values of 3 independent experiments ± SEM. *$P < .05$, **$P < .01$, and ***$P < .001$ versus control as determined by Student unpaired *t* test. (G-I) RLEC proliferation induced by 72-hour exposure to VEGF-C152S (25-200 ng/mL; G), IL-3 (5-100 ng/mL; H), and LPS (50-1000 ng/mL; I). (J) Additive proliferative effects of RLECs treated with VEGF-C152S (100 ng/mL), IL-3 (10 ng/mL), or LPS (500 ng/mL) alone compared with pretreatment with IL-3 (10 ng/mL) or LPS (500 ng/mL) followed by stimulation with VEGF-C152S (100 ng/mL). (G-J) Data are presented as the average cell number of 3 independent experiments ± SEM (total n = 6 per condition). (K) Migration of RLECs induced by treatment with VEGF-C152S (200 ng/mL), IL-3 (10 ng/mL), or LPS (500 ng/mL) and combined treatment with IL-3 (10 ng/mL) and VEGF-C152S (200 ng/mL) or LPS (500 ng/mL) and VEGF-C152S (200 ng/mL). RLEC migration toward 0.25% FBS was used as a negative control. Data presented as average fold increase in RLEC migration ± SEM of 3 independent experiments. (J-K) *$P < .05$, **$P < .01$, and ***$P < .001$ versus control. ##$P < .01$ and ###$P < .001$ versus cytokine treatment alone. +$P < .05$, ++$P < .01$, and +++$P < .001$ versus VEGF-C152S treatment alone. All statistical tests were done by Student unpaired *t* test.

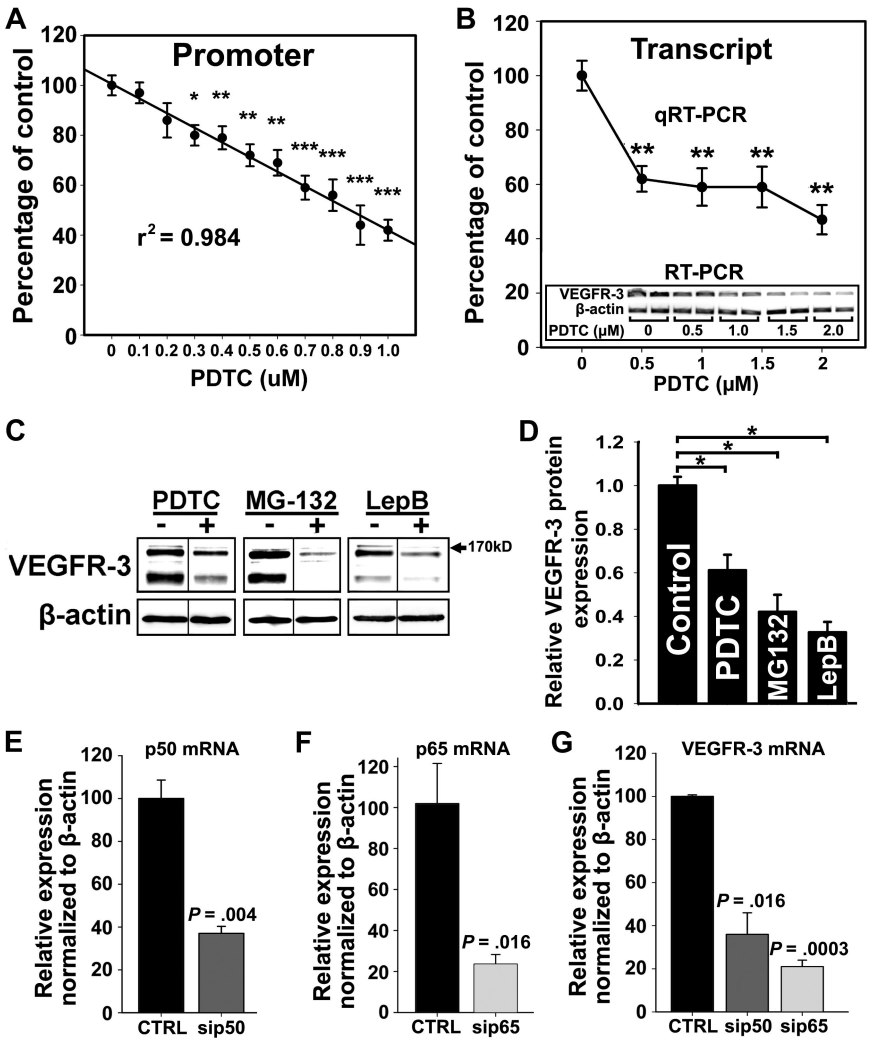

Figure 5. NF-κB signaling is required for VEGFR-3 expression in lymphatic endothelial cells. (A) RLECs were transfected with the full-length VEGFR-3$^{-849/+55}$ promoter and treated with PDTC (0-1μM) or vehicle for 18 hours. Promoter activity was measured by luciferase assay and normalized to total protein per well. Note linear inhibition of VEGFR-3 promoter activity by PDTC determined by linear regression (r^2 shown on graph) of the mean promoter activity ± SEM of 3 independent experiments performed in duplicate (total n = 6 per condition). (B) VEGFR-3 transcript expression assayed by qRT-PCR in RLECs treated with PDTC (0-2μM) or vehicle. Data are presented as mean transcript expression normalized to β-actin of 3 independent experiments ± SEM (total n = 3 per condition). Inset shows a dose-dependent decrease of VEGFR-3 transcript detected by RT-PCR. (B-C) *$P < .05$ versus control, **$P < .01$ versus control, ***$P < .001$ versus control, by Student unpaired *t* test. (C) Western blot analysis of RLECs treated with PDTC (7.5μM), MG-132 (0.25μM), leptomycin B (10nM), or vehicle for 24 hours. β-Actin was used as a loading control. Vertical lines have been inserted to indicate repositioned gel lanes from blots presented in supplemental Figure 6, which show dose-dependent responses to NF-κB inhibitors. (D) Densitometric values demonstrate a statistically significant decrease in VEGFR-3 protein normalized to β-actin from RLECs treated with NF-κB inhibitors or vehicle for 24 hours. Experiments were performed in duplicate and data are presented as mean normalized per β-actin VEGFR-3 expression ± SEM; *$P < .05$ versus control, by Student unpaired *t* test. (E-G) H-LLY cells were transfected with p50- or p65-specific siRNA or scramble control siRNA for 48 hours and transcript expression for p50 (E), p65 (F), and VEGFR-3 (G) was determined by qRT-PCR. Data are presented as the mean transcript expression normalized to β-actin of 3 independent samples ± SEM (n = 3 per condition). Statistically significant differences were determined versus control, by Student unpaired *t* test. *P* values are displayed on the graphs.

Inhibition of NF-κB signaling represses VEGFR-3 expression in LECs

Because VEGFR-3 was elevated in inflamed lymphatic vessels (Figures 1-2) and upon forced expression of NF-κB proteins (Figure 4), we hypothesized that endogenous VEGFR-3 expression in LECs is maintained by constitutive NF-κB signaling. To test this hypothesis, we determined the effects of an NF-κB inhibitor PDTC[40] on VEGFR-3 expression at promoter, mRNA, and protein levels. PDTC-treated LECs demonstrated a dose-dependent reduction (up to 60%) of VEGFR-3 promoter activity and mRNA (Figure 5A-B). Constitutive expression and nuclear localization of p50 and p65 were also inhibited by PDTC, which coincided with decreased VEGFR-3 expression (supplemental Figure 5). Neither cell viability (supplemental Figure 6) nor expression of NF-κB–independent targets (eg, β-actin) was affected by PDTC at the tested concentrations (Figure 5B inset). This effect was reproduced by 2 other inhibitors: MG-132, a blocker of IκB-α degradation,[40] and leptomycin B, an inhibitor of NF-κB nuclear transport.[41] Western blot showed up to 70% reduction of VEGFR-3 expression by all inhibitors in a dose-dependent manner (Figure 5C-D). Drug concentrations that repressed VEGFR-3 protein expression were at least 10-fold below the median inhibitory concentration values for LECs (supplemental Figure 6).

NF-κB regulation of VEGFR-3 expression was also confirmed by target-specific knockdown of NF-κB subunits. H-LLY cells were transfected with siRNA targeting p50 or p65 or scrambled control siRNA. qRT-PCR performed 48 hours after transfection showed 50% to 70% knockdown of p50 and p65 (Figure 5E-F) and a corresponding 50% to 80% reduction in VEGFR-3 transcripts (Figure 5G). Collectively, these data suggest that NF-κB is involved in regulation of endogenous VEGFR-3 expression.

The VEGFR-3 promoter is activated by Prox1

Prox1 has been reported to induce VEGFR-3 expression in cultured endothelial cells.[18,20] However, Prox1 regulates more than 90 genes[20] and transactivation of the VEGFR-3 promoter by Prox1 has not been previously shown. To determine whether Prox1 transcriptionally regulates VEGFR-3, LECs were cotransfected with VEGFR-3$^{-849/+55}$ promoter and escalating concentrations (0-0.5 μg) of a Prox1-encoding or empty vector followed by measurement of luciferase activity. Relative to empty-vector control, overexpression of Prox1 increased VEGFR-3$^{-849/+55}$ activity in a linear dose-dependent manner by 76-fold and 7-fold in H-LLY and RLECs, respectively (Figure 6A-B).

Several putative Prox1 binding sites, analogous to published consensus sequences (CA/tc/tNNCT/c and TA/tAGNC/tN[42]), are present in both human and rat VEGFR-3 promoters. ChIP assay in RLECs showed that the region containing consensus Prox1 binding sites (−403/−238 bp) was immunoprecipitated by anti-Prox1 antibody (Figure 6C, supplemental Figure 7). Prox1 antibodies did

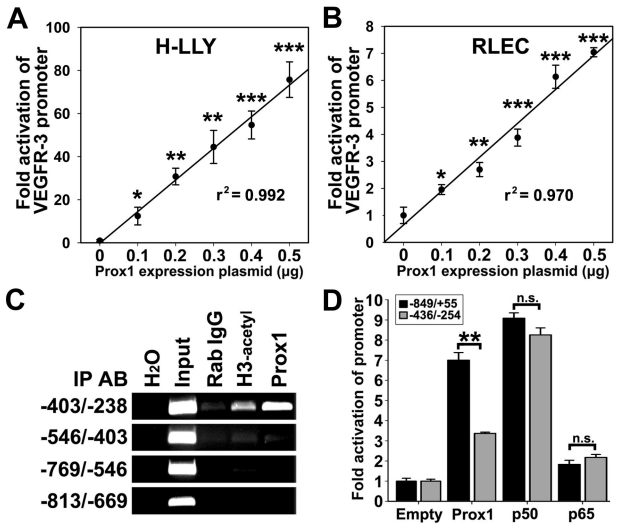

Figure 6. Prox1 directly activates the VEGFR-3 promoter. VEGFR-3$^{-849/+55}$ promoter plasmid was cotransfected with pCMV-Prox1 plasmid (0-0.5 μg) in H-LLY cells (A) and RLECs (B). Promoter activity was measured by luciferase assay and normalized per milligram of protein. Note linear response to Prox1 transactivation in both cell lines as determined by linear regression (r^2 shown on graph) of the mean promoter activity ± SEM of 3 independent experiments performed in duplicate (n = 6 per condition; A-B). (A-B) *$P < .05$ versus control, **$P < .01$ versus control, ***$P < .001$ versus control, by Student unpaired *t* test. (C) ChIP analysis of the VEGFR-3 promoter was performed on RLECs as described in the legend for Figure 4. Immunoprecipitated chromatin was visualized by PCR with primers flanking transcription factor binding sites (−403/−238 bp) or upstream of binding sites (−813/−403 bp). Data are representative of 3 independent ChIP experiments with similar results. (D) Fold activation of a truncated VEGFR-3 promoter (−436/−254) was compared with the full-length VEGFR-3$^{-849/+55}$. RLECs were cotransfected with 0.5 μg of VEGFR-3$^{-849/+55}$ or VEGFR-3$^{-436/-254}$ promoter plasmids and 0.5 μg of pCMV-Prox1, pCMV-Flag-p50, pCMV-Flag-p65, or empty control plasmid. Promoter activity is normalized per milligram of protein. Data are presented as the mean promoter activity of 3 independent experiments performed in duplicate ± SEM (total n = 6 per experimental condition). ns denotes nonsignificant changes. **$P < .01$ versus control as determined by Student unpaired *t* test.

not pull down other flanking promoter DNA, indicating specific interaction between Prox1 and the VEGFR-3 promoter within a promoter segment that was also bound by NF-κB (Figure 4B). To test whether this region is crucial for promoter activation, RLECs were cotransfected with a construct encoding bases −436 to −254 (VEGFR-3$^{-436/-254}$) and pCMV-Prox1, pCMV-Flag-p50, pCMV-Flag-p65, or empty plasmids. VEGFR-3$^{-849/+55}$ and VEGFR-3$^{-436/-254}$ were identically activated by p50 and p65, whereas Prox1 fold activation of VEGFR-3$^{-436/-254}$ was reduced approximately by half compared with the full-length promoter (Figure 6D). This suggests that full activation by Prox1 might require interaction with additional sites outside of the −436/−254-bp region.

NF-κB regulates Prox1 expression in LECs

We found that forced expression of Prox1 activated VEGFR-3 promoter in vitro and both Prox1 and VEGFR-3 are induced by inflammation in vivo with Prox1 up-regulation preceding that of VEGFR-3 (Figure 2). This suggested that NF-κB might first up-regulate Prox1 followed by cooperative regulation of VEGFR-3. To test this hypothesis, the level of Prox1 expression was quantified by qRT-PCR after 6-hour stimulation by IL-3 (10 ng/mL), conditions that increased VEGFR-3 expression (Figure 4E). IL-3 significantly increased Prox1 by 2-fold ($P < .01$, Figure 7A), implicating Prox1 as a downstream target of NF-κB.

We next investigated the effects of NF-κB inhibitors on Prox1 expression. PDTC suppressed Prox1 mRNA by approximately 60% (Figure 7B), suggesting that Prox1 transcription requires NF-κB. Western blot showed that PDTC, MG-132, and leptomycin B all significantly repressed Prox1 expression (Figure 7C). Moreover, p50 and p65 siRNA but not scrambled control also decreased Prox1 expression by 60% (Figure 7D), corroborating the hypothesis that NF-κB regulates Prox1 in LECs.

Prox1 and NF-κB synergistically activate the VEGFR-3 promoter

Cultured LECs express high levels of Prox1 and p50, making it difficult to evaluate the contributions of these factors to VEGFR-3 transcription. To test whether Prox1 and NF-κB cooperate in activation of the VEGFR-3 promoter, we used Prox1-negative nonendothelial (HEK293) and endothelial (HULEC) lines. Similar results were obtained in both lines cotransfected with Prox1 (Figure 7E-F insets), the full-length VEGFR-3$^{-849/+55}$ promoter and Flag-p50, Flag-p65, or empty vector. In the absence of Prox1, p50 weakly activated the VEGFR-3 promoter, whereas p65 had no effect. Prox1 combined with p65 did not increase promoter activity compared with Prox1 alone. In contrast, Prox1 combined with p50 activated the VEGFR-3 promoter 22.3-fold (± 0.7-fold) and 66.9-fold (± 3.8-fold) over the vector control in HEK293 cells and HULECs, respectively (Figure 7E-F). Combination of these plasmids had no effect on the activity of NF-κB–independent ubiquitin C (UBC) or phosphoglycerate kinase (PGK) promoters. The activity of a truncated VEGFR-3$^{-118/+55}$ promoter in response to Prox1, p50, and p65 alone or in combination was significantly reduced compared with the responses of the full-length VEGFR-3$^{-849/+55}$ (Figure 7G, supplemental Figure 8). These results confirm the functionality of the region beyond −118 bp and suggest that Prox1 and NF-κB p50 synergistically activate the VEGFR-3 promoter.

Discussion

Inflammation and NF-κB signaling up-regulate VEGFR-3 expression during lymphangiogenesis

Inflammation is the main physiologic event that evokes formation of new lymphatic vessels in adulthood.[43] Although the role of inflammation in induction of lymphangiogenesis has long been recognized, the underlying molecular mechanisms remained undefined. We present novel evidence that inflammation-induced NF-κB signaling precedes lymphatic-specific up-regulation of VEGFR-3 and that NF-κB activates VEGFR-3 transcription in cultured LECs (Figures 1-2,4). Moreover, our data show that NF-κB–dependent mediators, IL-3 and LPS, increase VEGFR-3 expression and responsiveness of LECs to VEGFR-3–activating factors (Figure 4). Collectively, these results suggest that LEC stimulation by NF-κB–dependent cytokines amplifies the lymphangiogenic signals by increasing VEGFR-3 expression.

In vivo analysis demonstrated that up-regulation of VEGFR-3 on preexisting vessels preceded formation of new LYVE-1$^+$ vessels by several days (Figures 1-2), suggesting that elevated VEGFR-3 expression is crucial for induction of lymphangiogenesis. This is consistent with previous reports demonstrating the paramount role of VEGFR-3 for LEC activation and inflammatory lymphangiogenesis as shown by blocking this receptor in models of LPS-induced peritonitis,[44] chronic airway infection,[9] wound healing,[16] and cancer.[17] VEGFR-3 ligands, VEGF-C/-D, are highly expressed during inflammation by infiltrating immune cells, such as CD11b$^+$ macrophages.[44,45] The abundant expression of VEGF-C/-D at inflamed sites suggests that lymphangiogenesis might be restricted by limited VEGFR-3 expression on preexisting

lymphatic vessels rather than by ligand availability. A low density of VEGFR-3 receptors may result in self-limiting lymphangiogenesis due to receptor saturation and internalization. In contrast, high level of VEGFR-3 expression might be induced by inflammation due to sustained cytokine production and continuous activation of NF-κB in LECs.

Prox1 is up-regulated during inflammation and mediates VEGFR-3 expression

Prox1 is an essential mediator of embryonic lymphangiogenesis,[18,20] but little is known about its functions in adulthood. We present novel evidence that Prox1 expression is rapidly increased after the onset of inflammation preceding both VEGFR-3 up-regulation and lymphangiogenesis (Figures 1-2). We also showed that the NF-κB–dependent cytokine, IL-3, up-regulates Prox1 in adult LECs, which is consistent with prior reports that IL-3 induced Prox1 expression in adult BECs.[22] Elevated expression of Prox1 and VEGFR-3 has also been shown in Kaposi sarcoma.[46] However, the latter finding could be construed as induction by tumor-derived factors rather than by sustained NF-κB activation. In comparison, we report here lymphatic-specific induction of Prox1 by NF-κB–dependent cytokines and suppression of Prox1 by NF-κB–specific inhibitors. These data suggest that Prox1 might regulate responsiveness to inflammation in adult LECs.

Prox1 regulates acquisition of lymphatic phenotype during embryogenesis[18] and transdifferentiation of adult BECs to LECs.[18,20] Up-regulation of Prox1 induces VEGFR-3,[18,20] whereas silencing Prox1 suppresses VEGFR-3 expression.[21] Our data suggest that Prox1 induces VEGFR-3 expression through promoter transactivation as indicated by ChIP and a dose-dependent increase in promoter activity (Figure 6). These data identify Prox1 as a potential downstream target of NF-κB and a regulator of VEGFR-3 expression under inflammatory conditions.

VEGFR-3 transcription is predominantly regulated by NF-κB p50 that might cooperate with Prox1

We show that NF-κB p50, rather than p65, is the predominant activator of VEGFR-3 (Figures 4,7). Preferential activation by p50 was reported for other promoters including Bcl-2[47] and PDGF-A.[48] In contrast, promoters of some NF-κB responsive genes (eg, TNF-α and IL-8) are suppressed by p50 homodimers.[49] This suggests that p50 can function as a transcriptional activator or repressor depending on cellular context, sequence of the response element, and transcriptional cofactors. Because p50 lacks a consensus transactivation domain,[24] p50-driven transcription requires coactivators, such as Bcl-3[47] or C/EBP proteins,[50] that might be present in LECs. Both Prox1 and p50 have been shown to interact with the transcriptional coactivator, CBP/p300,[50] suggesting that such protein-protein interaction might account for synergistic activation of the VEGFR-3 promoter (Figure 7). Prox1 might also

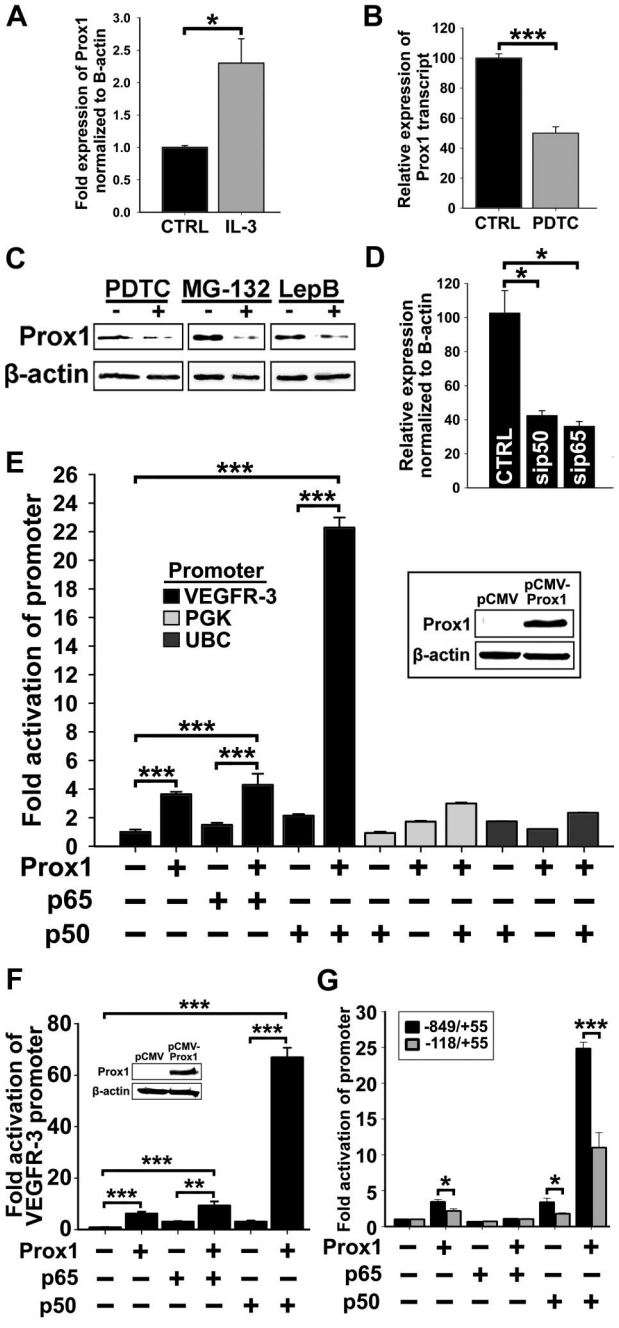

Figure 7. The p50 subunit of NF-κB up-regulates Prox1, and both p50 and Prox1 synergistically regulate VEGFR-3 expression. (A) qRT-PCR analysis of Prox1 transcripts in HDLECs$_{htert}$ treated with IL-3 (10 ng/mL) for 6 hours. (B) qRT-PCR analysis of Prox1 transcripts in RLECs treated with PDTC (2.5μM) for 24 hours. (A-B) Data are presented as β-actin normalized mean transcript expression of 3 independent experiments performed in duplicate ± SEM (total: n = 6 per condition). (C) Prox1 detected by Western blot of nuclear extracts from RLECs treated with PDTC (5μM), MG-132 (250nM), leptomycin B (10nM), or vehicle alone. β-Actin was used as a loading control. Representative data are shown from 1 of 3 experiments. (D) qRT-PCR analysis of Prox1 transcript in H-LLY transfected with p50 and p65 siRNA. Data are presented as the mean transcript expression normalized to β-actin ± SEM derived from 3 independent samples. (E) Prox1-negative nonendothelial line HEK293 was transfected with VEGFR-3$^{-849/+55}$ promoter plasmid and pCMV-Flag-p50 or pCMV-Flag-p65 plasmids and cotransfected with pCMV-Prox1 or empty vector (0.25 μg of each plasmid). VEGFR-3 promoter activity was normalized to total milligram of protein. Inset confirms lack of Prox1 in control HEK293 and forced expression in transfected cells. Activation of VEGFR-3 promoter by coexpression of p50 and Prox1 was compared with the effect on NF-κB–independent promoters for phosphoglycerate kinase (PGK) and ubiquitin C (UBC) examined under the same conditions. Data presented as the mean promoter activity ± SEM of 3 independent experiments performed in triplicate (total n = 9 per condition). (F) Prox1-negative blood vascular endothelial line, HULEC, was transfected with VEGFR-3$^{-849/+55}$ promoter expression and pCMV-Flag-p50 or pCMV-Flag-p65 plasmids and cotransfected with pCMV-Prox1 or empty vector, as described in panel E. The analysis of the VEGFR-3 promoter activity was performed as described in panel E. Data are presented as the mean VEGFR-3 promoter activity ± SEM derived from 3 independent experiments performed in quadruplicate (total n = 12 per condition). (G) Fold activation of the full-length (−849/+55 bp) and truncated (−118/+55 bp) VEGFR-3 promoters was compared after cotransfection with pCMV-Prox1, pCMV-Flag-p50, and pCMV-Flag-p65 alone or in combination as described in panel E. Data are presented as the mean VEGFR-3 promoter activity ± SEM derived from 3 independent experiments. *$P < .05$, **$P < .01$, and ***$P < .001$ versus control, as determined by Student unpaired *t* test.

be a lymphatic-specific coactivator of p50, which would account for the weak transactivation of the VEGFR-3 promoter by p50 in Prox1-negative BECs (Figure 7) and the lack of VEGFR-3 up-regulation on inflamed blood vasculature (supplemental Figure 3). This is consistent with overlapping peaks and protein kinetics of p-p50 and Prox1 observed in vivo (Figure 2), suggesting that Prox1 might confer lymphatic specificity to ubiquitously activated NF-κB signaling during inflammation. Thus, the cooperative role of Prox1 with p50 in regulation of VEGFR-3 transcription could be 2-fold: to amplify p50 signaling and to impart lymphatic specificity to activated NF-κB, promoting lymphangiogenesis-required gene expression.

In summary, we demonstrate that increased Prox1 and VEGFR-3 expression precedes lymphangiogenesis in vivo. Increased expression of VEGFR-3 is likely mediated by Prox1 and NF-κB binding to its promoter. Prox1 induced by NF-κB synergizes with p50 in activation of the promoter, suggesting a complex interplay between ubiquitous and lymphatic-specific proteins. Future delineation of these mechanisms might identify targets for therapeutic control of abnormal lymphangiogenesis induced at chronically inflamed sites and malignancy.

Acknowledgments

We thank Dr Albert Baldwin and Stephen Markwell for providing NF-κB plasmids and statistical data analysis, respectively. We also thank Lisa Volk and Kathleen Brancato for assistance with animal experiments and immunostaining, respectively.

This study was funded, in part, by the National Institutes of Health (no. 1R15CA125682-01), Illinois William E. McElroy Foundation and SIUSOM Excellence in Medicine awards (S.R.), and by a Department of Defense Breast Cancer Research Program predoctoral traineeship (no. BC073318; M.J.F.).

Authorship

Contribution: M.J.F. designed research, performed or supervised experiments, analyzed and interpreted data, and wrote the paper; A.W. contributed vital new reagents and wrote the paper; K.L.H. performed siRNA experiments; C.I. and K.M. contributed vital new reagents; R.E.N. and M.S.P. contributed HDLECs$_{htert}$; D.C.Z. contributed RLECs; and S.R. designed research, supervised experiments, analyzed and interpreted data, and wrote the paper.

Conflict-of-interest disclosure: The authors declare no competing financial interests.

Correspondence: Sophia Ran, Department of Medical Microbiology, Immunology and Cell Biology, Southern Illinois University School of Medicine, 801 N Rutledge, Springfield, IL 62794-9626; e-mail: sran@siumed.edu.

References

1. Swartz MA, Hubbell JA, Reddy ST. Lymphatic drainage function and its immunological implications: from dendritic cell homing to vaccine design. *Semin Immunol.* 2008;20(2):147-156.
2. Shin WS, Rockson SG. Animal models for the molecular and mechanistic study of lymphatic biology and disease. *Ann N Y Acad Sci.* 2008; 1131:50-74.
3. Jamieson T, Cook DN, Nibbs RJ, et al. The chemokine receptor D6 limits the inflammatory response in vivo. *Nat Immunol.* 2005;6(4):403-411.
4. Achen MG, Stacker SA. Molecular control of lymphatic metastasis. *Ann N Y Acad Sci.* 2008;1131: 225-234.
5. Veikkola T, Jussila L, Makinen T, et al. Signalling via vascular endothelial growth factor receptor-3 is sufficient for lymphangiogenesis in transgenic mice. *EMBO J.* 2001;20(6):1223-1231.
6. Kaipainen A, Korhonen J, Mustonen T, et al. Expression of the fms-like tyrosine kinase 4 gene becomes restricted to lymphatic endothelium during development. *Proc Natl Acad Sci U S A.* 1995;92(8):3566-3570.
7. Whitehurst B, Flister MJ, Bagaitkar J, et al. Anti-VEGF-A therapy reduces lymphatic vessel density and expression of VEGFR-3 in an orthotopic breast tumor model. *Int J Cancer.* 2007;121(10): 2181-2191.
8. Paavonen K, Puolakkainen P, Jussila L, Jahkola T, Alitalo K. Vascular endothelial growth factor receptor-3 in lymphangiogenesis in wound healing. *Am J Pathol.* 2000;156(5):1499-1504.
9. Baluk P, Tammela T, Ator E, et al. Pathogenesis of persistent lymphatic vessel hyperplasia in chronic airway inflammation. *J Clin Invest.* 2005; 115(2):247-257.
10. Kunstfeld R, Hirakawa S, Hong YK, et al. Induction of cutaneous delayed-type hypersensitivity reactions in VEGF-A transgenic mice results in chronic skin inflammation associated with persistent lymphatic hyperplasia. *Blood.* 2004;104(4): 1048-1057.
11. Zhang Q, Lu Y, Proulx ST, et al. Increased lymphangiogenesis in joints of mice with inflammatory arthritis. *Arthritis Res Ther.* (http://arthritis-research.com/content/pdf/ar2326.pdf). 2007;9(6): R118.
12. Maruyama K, Ii M, Cursiefen C, et al. Inflammation-induced lymphangiogenesis in the cornea arises from CD11b-positive macrophages. *J Clin Invest.* 2005;115(9):2363-2372.
13. Cursiefen C, Chen L, Borges LP, et al. VEGF-A stimulates lymphangiogenesis and hemangiogenesis in inflammatory neovascularization via macrophage recruitment. *J Clin Invest.* 2004; 113(7):1040-1050.
14. Iwata C, Kano MR, Komuro A, et al. Inhibition of cyclooxygenase-2 suppresses lymph node metastasis via reduction of lymphangiogenesis. *Cancer Res.* 2007;67(21):10181-10189.
15. Ristimäki A, Narko K, Enholm B, Joukov V, Alitalo K. Proinflammatory cytokines regulate expression of the lymphatic endothelial mitogen vascular endothelial growth factor-C. *J Biol Chem.* 1998; 273(14):8413-8418.
16. Goldman J, Rutkowski JM, Shields JD, et al. Cooperative and redundant roles of VEGFR-2 and VEGFR-3 signaling in adult lymphangiogenesis. *FASEB J.* 2007;21(4):1003-1012.
17. Roberts N, Kloos B, Cassella M, et al. Inhibition of VEGFR-3 activation with the antagonistic antibody more potently suppresses lymph node and distant metastases than inactivation of VEGFR-2. *Cancer Res.* 2006;66(5):2650-2657.
18. Hong YK, Harvey N, Noh YH, et al. Prox1 is a master control gene in the program specifying lymphatic endothelial cell fate. *Dev Dyn.* 2002; 225(3):351-357.
19. Wigle JT, Harvey N, Detmar M, et al. An essential role for Prox1 in the induction of the lymphatic endothelial cell phenotype. *EMBO J.* 2002;21(7): 1505-1513.
20. Petrova TV, Makinen T, Makela TP, et al. Lymphatic endothelial reprogramming of vascular endothelial cells by the Prox-1 homeobox transcription factor. *EMBO J.* 2002;21(17):4593-4599.
21. Mishima K, Watabe T, Saito A, et al. Prox1 induces lymphatic endothelial differentiation via integrin alpha9 and other signaling cascades. *Mol Biol Cell.* 2007;18(4):1421-1429.
22. Gröger M, Loewe R, Holnthoner W, et al. IL-3 induces expression of lymphatic markers Prox-1 and podoplanin in human endothelial cells. *J Immunol.* 2004;173(12):7161-7169.
23. Karin M. Nuclear factor-kappaB in cancer development and progression. *Nature.* 2006;441(7092):431-436.
24. Beinke S, Ley SC. Functions of NF-kappaB1 and NF-kappaB2 in immune cell biology. *Biochem J.* 2004;382(pt 2):393-409.
25. Kiriakidis S, Andreakos E, Monaco C, et al. VEGF expression in human macrophages is NF-kappaB-dependent: studies using adenoviruses expressing the endogenous NF-kappaB inhibitor IkappaBalpha and a kinase-defective form of the IkappaB kinase 2. *J Cell Sci.* 2003; 116(pt 4):665-674.
26. Tsai PW, Shiah SG, Lin MT, Wu CW, Kuo ML. Up-regulation of vascular endothelial growth factor C in breast cancer cells by heregulin-beta 1: a critical role of p38/nuclear factor-kappa B signaling pathway. *J Biol Chem.* 2003;278(8):5750-5759.
27. Wilber A, Frandsen JL, Wangensteen KJ, et al. Dynamic gene expression after systemic delivery of plasmid DNA as determined by in vivo bioluminescence imaging. *Hum Gene Ther.* 2005;16(11): 1325-1332.
28. Whitehurst B, Eversgerd C, Flister M, et al. Molecular profile and proliferative responses of rat lymphatic endothelial cells in culture. *Lymphat Res Biol.* 2006;4(3):119-142.
29. Nisato RE, Harrison JA, Buser R, et al. Generation and characterization of telomerase-transfected human lymphatic endothelial cells with an extended life span. *Am J Pathol.* 2004; 165(1):11-24.
30. Tammela T, Saaristo A, Lohela M, et al. Angiopoietin-1 promotes lymphatic sprouting and hyperplasia. *Blood.* 2005;105(12):4642-4648.
31. National Center for Biotechnology Information. GenBank. http://www.ncbi.nlm.nih.gov/Genbank. Accessed February 14, 2007.

32. Genomatix. MatInspector. http://www.genomatix.de/products/MatInspector/index.html. Accessed March 02, 2007.
33. Laderach D, Compagno D, Danos O, Vainchenker W, Galy A. RNA interference shows critical requirement for NF-kappa B p50 in the production of IL-12 by human dendritic cells. *J Immunol.* 2003;171(4):1750-1757.
34. Surabhi RM, Gaynor RB. RNA interference directed against viral and cellular targets inhibits human immunodeficiency virus type 1 replication. *J Virol.* 2002;76(24):12963-12973.
35. Kilic N, Oliveira-Ferrer L, Neshat-Vahid S, et al. Lymphatic reprogramming of microvascular endothelial cells by CEA-related cell adhesion molecule-1 via interaction with VEGFR-3 and Prox1. *Blood.* 2007;110(13):4223-4233.
36. Oka M, Iwata C, Suzuki HI, et al. Inhibition of endogenous TGF-{beta} signaling enhances lymphangiogenesis. *Blood.* 2008;111(9):4571-4579.
37. Srinivasan RS, Dillard ME, Lagutin OV, et al. Lineage tracing demonstrates the venous origin of the mammalian lymphatic vasculature. *Genes Dev.* 2007;21(19):2422-2432.
38. Iljin K, Karkkainen MJ, Lawrence EC, et al. VEGFR3 gene structure, regulatory region, and sequence polymorphisms. *FASEB J.* 2001;15(6):1028-1036.
39. Kirkin V, Mazitschek R, Krishnan J, et al. Characterization of indolinones which preferentially inhibit VEGF-C- and VEGF-D-induced activation of VEGFR-3 rather than VEGFR-2. *Eur J Biochem.* 2001;268(21):5530-5540.
40. Dai Y, Rahmani M, Grant S. Proteasome inhibitors potentiate leukemic cell apoptosis induced by the cyclin-dependent kinase inhibitor flavopiridol through a SAPK/JNK- and NF-kappaB-dependent process. *Oncogene.* 2003;22(46):7108-7122.
41. Walsh MD Jr, Hamiel CR, Banerjee A, et al. Exportin 1 inhibition attenuates nuclear factor-kappaB-dependent gene expression. *Shock.* 2008;29(2):160-166.
42. Chen X, Taube JR, Simirskii VI, Patel TP, Duncan MK. Dual roles for Prox1 in the regulation of the chicken betaB1-crystallin promoter. *Invest Ophthalmol Vis Sci.* 2008;49(4):1542-1552.
43. Mouta C, Heroult M. Inflammatory triggers of lymphangiogenesis. *Lymphat Res Biol.* 2003;1(3):201-218.
44. Kataru RP, Jung K, Jang C, et al. Critical role of CD11b+ macrophages and VEGF in inflammatory lymphangiogenesis, antigen clearance, and inflammation resolution. *Blood.* 2009;113(22):5650-5659.
45. Kang S, Lee SP, Kim KE, et al. Toll-like receptor 4 in lymphatic endothelial cells contributes to LPS-induced lymphangiogenesis by chemotactic recruitment of macrophages. *Blood.* 2009;113(11):2605-2613.
46. Hong YK, Foreman K, Shin JW, et al. Lymphatic reprogramming of blood vascular endothelium by Kaposi sarcoma-associated herpesvirus. *Nat Genet.* 2004;36(7):683-685.
47. Kurland JF, Kodym R, Story MD, et al. NF-kappaB1 (p50) homodimers contribute to transcription of the bcl-2 oncogene. *J Biol Chem.* 2001;276(48):45380-45386.
48. Aizawa K, Suzuki T, Kada N, et al. Regulation of platelet-derived growth factor-A chain by Kruppel-like factor 5: new pathway of cooperative activation with nuclear factor-kappaB. *J Biol Chem.* 2004;279(1):70-76.
49. Tong X, Yin L, Washington R, Rosenberg DW, Giardina C. The p50-p50 NF-kappaB complex as a stimulus-specific repressor of gene activation. *Mol Cell Biochem.* 2004;265(1-2):171-183.
50. Chen Q, Dowhan DH, Liang D, Moore DD, Overbeek PA. CREB-binding protein/p300 coactivation of crystallin gene expression. *J Biol Chem.* 2002;277(27):24081-24089.

Appendix B

MATERIALS AND METHODS

Antibodies

Goat anti-mVEGFR-3 and anti-Prox1 antibodies were purchased from R&D Systems (Minneapolis, MN). Rabbit anti-mLYVE-1 and anti-Prox1 antibodies were purchased from AngioBio (Del Mar, CA). MECA-32, a pan anti-mouse vascular endothelial cell antibody, was purchased from Developmental Studies Hybridoma Bank (Iowa City, IA). Secondary donkey anti-rabbit, anti-goat, and anti-rat antibodies conjugated with DyLight 488 or DyLight 549 were purchased from Jackson ImmunoResearch Laboratories (West Grove, PA).

Animals

Female B6129PF2/J (F2) ($p50^{+/+}$) and B6;129P2-Nfkb 1<tm 1 Bal> ($p50^{-/-}$) mice 4-6 weeks of age were obtained from the Jackson Laboratory (Bar Harbor, ME) and treated in accordance with institutional guidelines set by the Animal Care and Use Committee at Southern Illinois University School of Medicine. Mice were anesthetized with a mixture of ketamine (Fort Dodge Animal Health, Fort Dodge, Iowa), xylazine (Phoenix Scientific Inc., St. Joseph, Missouri) and sterile water. Prior to tissue harvesting, fully anesthetized mice were perfused with 5mM $CaCl_2$ solution. Harvested tissues were snap-frozen in liquid nitrogen and then fixed in Shandon Cryomatrix (Thermo Scientific, Waltham, MA) for cryostat sectioning.

Immunofluorescent staining

Frozen sections were fixed with acetone for 10 minutes, washed in PBST (pH 7.4, 0.1% Tween-20) for 10 minutes and incubated for 2 hours at 37°C with primary antibodies (diluted 1:100 in PBST containing 5 µg/ml BSA) against VEGFR-3, LYVE-1, Prox1, or MECA-32, followed by appropriate DyLight 488- or 549-conjugated secondary antibodies (diluted 1:100 in PBST containing 5 µg/ml BSA) for 1 hour at 37°C. For double immunofluorescent staining, sections were incubated with primary for 2 hours at 37°C, followed by secondary antibody for 1 hour at 37°C, with a wash for 10 minutes in PBST between steps. Slides were mounted in Vectashield medium containing 4,6'-diamidino-2-phenylindole (DAPI) nuclear stain (Vector Labs, Orton Southgate, U.K.). Images were acquired on an Olympus BX41 upright microscope equipped with a DP70 digital camera and DP Controller software (Olympus, Center Valley, PA).

Quantification of vessel density

Frozen sections of wild type and knockout organs were acetone-fixed for 10 minutes and stained with antibody against the lymphatic-specific marker, LYVE-1 [49], for 1 hour at 37°C, followed by incubation with DyLight 488-conjugated donkey anti-rabbit secondary antibodies for 1 hour at 37°C. To quantify LYVE-1 positive vessel density, 3-4 representative images per organ were acquired at 100X, 200X, or 400X magnifications for lungs, MFP, and liver, respectively, and the total number of positive vessels was enumerated and normalized per area of the field (mm^2). Lymphatic vessel density is presented as the average number of LYVE-1 positive vessels per area of the field ± SEM (n = 3-5 mice per group).

Measurement of mean vascular area

The mean vascular area of LYVE-1 positive staining per field was calculated as described previously [38], with slight modifications. Briefly, frozen sections were stained with rabbit anti-mLYVE-1 or goat anti-mVEGFR-3 primary antibodies and DyLight 549-conjugated donkey anti-rabbit or donkey anti-goat secondary antibodies, as described above. Fluorescent images were acquired at a constant exposure time at 200X and 400X magnifications for MFP and liver sections, respectively. Images were acquired on an Olympus BX41 upright microscope equipped with a DP70 digital camera and DP Controller software (Olympus, Center Valley, PA). Colored images were sequentially converted to 8-bit grayscale and then to a binary image using Image J software (http://rsbweb.nih.gov/ij/). The total area of LYVE-1 positive staining was then calculated using the analyze particles function of Image J that was set to measure the area of positive staining greater then 10 pixels in size to exclude any background staining. Mean vascular areas were calculated from 3 images per section ± SEM (n = 3-5 mice per group).

Measurement of mean fluorescent intensity

The mean fluorescent intensity (MFI) of VEGFR-3 and Prox1 positive staining was calculated as described previously [50], with slight modifications. Briefly, frozen sections were stained with goat anti-mVEGFR-3 or goat anti-Prox1 antibodies, followed by incubation with DyLight 549-conjugated donkey anti-goat secondary antibodies as described above. Fluorescent images were acquired at a constant exposure time at 400X magnification on an Olympus BX41 upright microscope equipped with a DP70 digital camera and DP Controller software (Olympus, Center Valley, PA). To exclude background staining, sections stained with secondary antibodies only were used to set the exposure time to below detectable level of background fluorescence. Digital RGB images acquired at a constant exposure time were converted to 8-bit grayscale.

The fluorescent intensity for each pixel was calculated using the histogram function of Image J that was set up in the linear intensity range of 0 to 255 arbitrary units. Staining with secondary antibodies alone resulted in background fluorescence less than 10 units on this scale. MFI was calculated as the sum of the number of pixels above background multiplied by the intensity level in the range of 10-255 and divided by the total pixel number with intensity above 10 units. MFI values were obtained from 3 images per section (n = 3-5 mice per group) and presented as MFI units ± SEM. To compare the global reduction in fluorescent intensities in p50 KO and WT mice, representative RGB images were converted to 8-bit grayscale and visualized using the 3D interactive surface plot function of Image J.

Quantitative RT-PCR analysis

Four micrograms of total RNA extracted by Tri-reagent was reverse transcribed using a RevertAid First Strand cDNA synthesis kit, according to the manufacturer's protocol (Fermentas, Burlington, Ontario, Canada). Primers for qRT-PCR were designed against mouse and human CDS of angiogenic and lymphangiogenic proteins found in the NCBI database. Specific primer sequences were chosen using the Harvard primer database website (http://pga.mgh.harvard.edu/primerbank/index.html). All primers were purchased as annealed oligos from Integrated DNA Technologies (Coralville, IA) and sequences of primers used in this study are listed in Table 1. Quantitative RT-PCR was performed using Brilliant II SYBR Green Master Mix (Stratagene, La Jolla, CA) and an ABI 7500 Real-Time PCR machine (Applied Biosystems, Foster City, CA) according to the manufacturer's protocol. A typical qRT-PCR reaction consisted of an initial denaturation step at 95°C for 5 minutes followed by 40 cycles of denaturation at 95°C for 15 seconds and annealing, extension, and reading at 60°C for 1 minute. A final melting curve for each primer was calculated by heating from 60 to 90°C. Data were normalized to β-actin and relative mRNA expression was determined using the ΔΔCt method as described previously [51].

Inflammatory cytokines and receptors qRT-PCR array

Two microgram of combined total MFP RNA from p50 KO and WT mice (n = 4 mice per group) was synthesized using a RevertAid First Strand cDNA synthesis kit, according to the manufacturer's protocol (Fermentas, Burlington, Ontario, Canada). Inflammatory gene expression was examined using a mouse inflammatory cytokines and receptors RT^2 Profiler PCR Array, according to the manufacturer's protocol (PAMM-011, SABiosciences, Fredrick, MD). Target gene expression was normalized to β-actin. Relative

changes in mRNA expression of p50 KO MFP compared with WT was determined using the ΔΔCt method as described previously [51]. Data are presented as the β-actin normalized relative expression of transcripts in p50 KO MFP (n = 4 mice) compared with WT (n = 4 mice).

Statistical analysis

Statistical analysis was performed using SAS software (SAS Institute, Inc., Cary, NC). All results are expressed as the mean ± SEM and statistical differences were assessed by unpaired Student's *t*-test. Statistical significance was defined as $P<0.05$.